HHS Public Access

Author manuscript

Cell Rep. Author manuscript; available in PMC 2018 August 15.

Published in final edited form as:

Cell Rep. 2018 July 03; 24(1): 209–223.e6. doi:10.1016/j.celrep.2018.05.088.

Remodeling of the Acetylproteome by SIRT3 Manipulation Fails to Affect Insulin Secretion or β Cell Metabolism in the Absence of Overnutrition

Brett S. Peterson[1,2], **Jonathan E. Campbell**[1,2,3], **Olga Ilkayeva**[1], **Paul A. Grimsrud**[1], **Matthew D. Hirschey**[1,2,3], and **Christopher B. Newgard**[1,2,3,4,*]

[1]Duke Molecular Physiology Institute and Sarah W. Stedman Nutrition and Metabolism Center, Duke University Medical Center, Durham, NC 27701, USA

[2]Department of Pharmacology and Cancer Biology, Duke University Medical Center, Durham, NC 27710, USA

[3]Department of Medicine, Division of Endocrinology, Metabolism, and Nutrition, Duke University Medical Center, Durham, NC 27710, USA

[4]Lead Contact

SUMMARY

SIRT3 is a nicotinamide adenine dinucleotide (NAD^+)- dependent mitochondrial protein deacetylase purported to influence metabolism through post-translational modification of metabolic enzymes. Fuel-stimulated insulin secretion, which involves mitochondrial metabolism, could be susceptible to SIRT3-mediated effects. We used CRISPR/Cas9 technology to manipulate SIRT3 expression in β cells, resulting in widespread SIRT3-dependent changes in acetylation of key metabolic enzymes but no appreciable changes in glucose- or pyruvate-stimulated insulin secretion or metabolomic profile during glucose stimulation. Moreover, these broad changes in the SIRT3-targeted acetylproteome did not affect responses to nutritional or ER stress. We also studied mice with global SIRT3 knockout fed either standard chow (STD) or high-fat and high-sucrose (HFHS) diets. Only when chronically fed HFHS diet do SIRT3 KO animals exhibit a modest reduction in insulin secretion. We conclude that broad changes in mitochondrial protein acetylation in response to manipulation of SIRT3 are not sufficient to cause changes in islet function or metabolism.

In Brief

*Correspondence: chris.newgard@duke.edu.

AUTHOR CONTRIBUTIONS

B.S.P., J.E.C., M.D.H., and C.B.N. designed the studies. B.S.P. and J.E.C. performed the experiments. P.A.G. performed the proteomics analyses. O.I. performed the metabolomics analyses. B.S.P. and C.B.N. wrote the paper. B.S.P., J.E.C., O.I., P.A.G., M.D.H., and C.B.N. edited the paper.

SUPPLEMENTAL INFORMATION

Supplemental Information includes two figures and four tables and can be found with this article online at https://doi.org/10.1016/j.celrep.2018.05.088.

CONFLICTS OF INTEREST

The authors declare no competing interests.

Peterson et al. report that ablation of SIRT3 in 832/13 β cells dramatically alters the mitochondrial acetylproteome but does not affect insulin secretion, metabolomic profile, or β cell survival. Moreover, SIRT3 knockout causes a modest reduction in insulin secretion in mice fed a high-fat and high-sucrose but not a standard chow diet.

Graphical Abstract

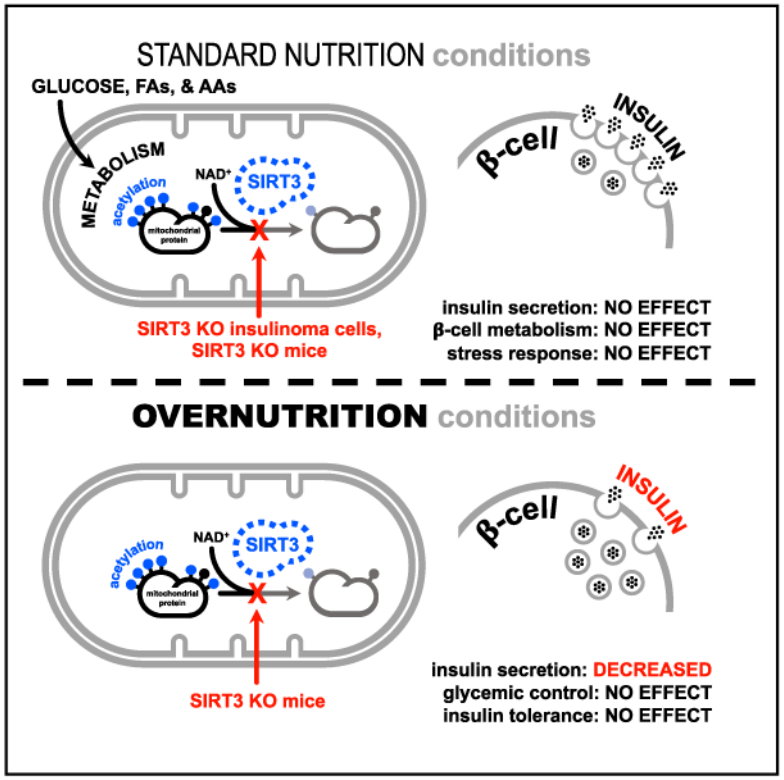

INTRODUCTION

Tight regulation of insulin secretion from pancreatic islet β cells in response to metabolic fuels and hormonal mediators is critical for systemic metabolic homeostasis. Indeed, loss of normal glucose-stimulated insulin secretion (GSIS) is a key component of the pathogenesis of type 2 diabetes (T2D) (Muoio and Newgard, 2008). Significant effort has been applied to develop strategies that protect and/or augment islet β cell function during the development of T2D, but the problem remains largely unsolved (Vetere et al., 2014). Therefore, continued efforts are needed to develop a more comprehensive understanding of the molecular mechanisms that affect GSIS and drive pathogenic β cell dysfunction.

GSIS is proportional to the rate of glucose metabolism and involves both oxidative and anaplerotic metabolism of glucosederived pyruvate in the mitochondria (Jensen et al., 2008, 2017; Muoio and Newgard, 2008; Prentki et al., 2013). Therefore, mitochondrial dysfunction has been proposed to contribute to the pathogenesis of β cell dysfunction in metabolic disease and T2D (Mulder, 2017), although the precise mechanisms remain

unclear. Similar to histones (Paik et al., 1970), mitochondrial proteins are thought to be nonenzymatically acetylated in the presence of acetyl-coenzyme A (CoA) (Davies et al., 2016; Wagner and Payne, 2013). A recent hypothesis proposes that nonenzymatic acetylation of lysine residues on mitochondrial proteins represents a “carbon stress” that promotes mitochondrial dysfunction (Wagner and Hirschey, 2014). In most cases, acetylation is purported to dampen the enzymatic activity of modified mitochondrial proteins (Baeza et al., 2016) and is, therefore, a presumed mechanism of impaired mitochondrial metabolism. Mammals express a mitochondrial deacetylase, Sirtuin-3 (SIRT3), that removes acetyl moieties from protein substrates to presumably restore their activity (Wagner and Hirschey, 2014). Taken together, this suggests that management of the SIRT3-targeted acetylproteome could affect β cell metabolism and, thus, the GSIS response. Further, disruption of this homeostatic mechanism under conditions of nutritional stress could contribute to β cell dysfunction.

Acetylation of mitochondrial proteins is increased in the liver in association with the development of metabolic dysfunction in 129Sv or C57BL/6 SVJ mice fed a high-fat “Western” diet (HFD) (Hirschey et al., 2011; Kendrick et al., 2011). Moreover, global SIRT3 knockout (SIRT3 KO) in 129Sv mice fed HFD results in exacerbated systemic metabolic dysregulation, suggesting that SIRT3-mediated deacetylation of mitochondrial proteins is a protective homeostatic mechanism during chronic overfeeding (Hirschey et al., 2011). Notably, after 3 months of HFD feeding, global SIRT3 KO mice exhibit significantly elevated plasma insulin levels in response to a glucose bolus (Hirschey et al., 2011), suggestive of SIRT3-mediated differences in the adaptive response of the β cell during chronic overfeeding.

Subsequent studies support a role for SIRT3 in the maintenance of β cell function (Caton et al., 2013; Kim et al., 2015; Zhang et al., 2016; Zhou et al., 2017). Knockdown of SIRT3 in β cell lines promotes both oxidative and endoplasmic reticulum (ER) stress, decreases cell viability, reduces glucose-stimulated ATP content, and, ultimately, impairs glucose- and leucine-stimulated insulin secretion (Caton et al., 2013; Zhang et al., 20616; Zhou et al., 2017). Pancreatic islets isolated from global SIRT3 KO 129Sv mice display increased markers of oxidative stress and apoptosis as well as impaired GSIS (Zhou et al., 2017). When cultured in elevated concentrations of fatty acids (FAs) to simulate the hyperlipidemic environment of the pancreatic islet in metabolic disease, β cell lines with suppressed SIRT3 expression are more vulnerable to fatty acid-induced impairment of GSIS (Zhang et al., 2016; Zhou et al., 2017). Supporting this observation, islets isolated from SIRT3 KO 129Sv mice fed HFD exhibit impaired GSIS (Zhou et al., 2017). Further, overexpression of SIRT3 reduces cell stress and preserves function in β cell lines and rat islets cultured in elevated glucose and fatty acids (Kim et al., 2015; Zhang et al., 2016; Zhou et al., 2017). The aforementioned studies suggest that SIRT3 plays a protective role in β cell health under a variety of conditions. However, these studies provide little or no data about changes in acetylation of specific proteins and also do not report changes in fuel metabolism in response to manipulation of SIRT3 expression. Thus, it is not currently possible to understand how changes in the SIRT3-targeted β cell acetylproteome might affect specific metabolic pathways that contribute to the regulation of insulin secretion and other islet functions.

To date, only glucose-regulated protein of 78 kDa (GRP78) and superoxide dismutase 2 (SOD2) have been shown to change acetylation state in response to SIRT3 manipulation in the β cell, leading to the assertion that acetylation of these two proteins regulates key β cell functions (Zhang et al., 2016; Zhou et al., 2017). However, it is unlikely that GRP78 and SOD2 are the only SIRT3-targeted proteins in the β cell, and there is no direct evidence that they regulate β cell function. Indeed, acetylproteomic analyses in other cell types and tissues reveals that the SIRT3-targeted acetylproteome includes enzymes in multiple metabolic pathways, such as fatty acid oxidation (FAO), the tricarboxylic acid (TCA) cycle, and the electron transport chain (ETC) (Dittenhafer-Reed et al., 2015; Hebert et al., 2013; Rardin et al., 2013; Sol et al., 2012). To evaluate potential links between SIRT3, mitochondrial protein acetylation, mitochondrial metabolism, and GSIS, we used the highly glucose-responsive INS-1 derived 832/13 β cell line (Hohmeier et al., 2000) and CRISPR/Cas9 technology to engineer complete SIRT3 KO β cells into which we stably integrated different SIRT3 transgenes. We have also expanded this work to include global SIRT3 KO mice, studied after chronic feeding of either standard chow (STD) or high-fat and high-sucrose (HFHS) diets. We show that manipulation of SIRT3 expression in β cell lines broadly and significantly alters the acetylation status of the mitochondrial acetylproteome but is not sufficient to alter fuel-stimulated insulin secretion, glucose metabolism, or responses to β cell stressinducing agents. The lack of effect of SIRT3-dependent changes in protein acetylation on islet function was confirmed in global SIRT3 KO mice fed STD diet. Chronic feeding of HFHS diet to global SIRT3 KO mice results in a modest reduction in insulin secretion, but these effects were not of sufficient magnitude to perturb glucose homeostasis.

RESULTS

Clonal Variability in 832/13 β Cell Subclones with Complete CRISPR/Cas9 D10A Mutant Nickase-Dependent Loss of SIRT3 Protein

We sought to understand how management of the SIRT3-targeted acetylproteome affects the function of pancreatic islet β cells. As our initial strategy, we tested several transfectable SIRT3-specific small interfering RNA (siRNA) oligonucleotides as well as a recombinant adenovirus containing a SIRT3-specific small hairpin RNA (shRNA) (Ad-shSIRT3) sequence. However, suppression of SIRT3 expression by these methods in the 832/13 β cell line revealed key obstacles. Suppression of SIRT3 protein expression was limited, such that several different targeting sequences (siRNA oligonucleotides or Ad-shSIRT3) suppressed SIRT3 protein by only 50% or less. This level of suppression was insufficient to cause measurable changes in the mitochondrial acetylproteome, as analyzed by immunoblot of mitochondrially enriched cellular subfractions with an anti-pan acetyllysine antibody. Different targeting sequences, despite similar suppression of SIRT3 expression, had significantly different effects on β cell function (data not shown).

We reasoned that the incomplete and transient knockdown of SIRT3 achieved with the siRNA or shRNA approach, possibly coupled with non-specific effects of the targeting sequences, contributed to the inconclusive findings regarding the role of the SIRT3-targeted acetylproteome in β cell function. To address these challenges, we applied a CRISPR/Cas9 gene-editing technique (Ran et al., 2013) to generate cell lines with complete, sustained, and

specific loss of the endogenous rat SIRT3 (rSIRT3) protein. 832/13 cells were transiently cotransfected with two plasmids containing the CRISPR/Cas9 D10A mutant nickase (Cas9n) enzyme and one of two unique pairs of chimeric guide RNA (gRNA) molecules targeting the *Rattus norvegicus Sirt3* gene. Following transient antibiotic selection and clonal expansion, complete and sustained loss of SIRT3 protein was confirmed in several 832/13 subclones by immunoblotting with a SIRT3-specific antibody (Figure 1A).

β Cell function was assessed by measuring GSIS. SIRT3 KO β cells were exposed to either a basal (2.8 mM) or stimulatory (16.7 mM) concentration of glucose for 2 hr, and insulin secretion was assayed by measuring its accumulation in the medium (Figures 1B–1D). GSIS was markedly different among several clones with complete SIRT3 ablation, again precluding clear conclusions. Based on the predicted specificity of the CRISPR/Cas9n system (Ran et al., 2013), we hypothesized that this functional heterogeneity might be a product of clonal variability. To test this, we derived new subclones (not subjected to CRISPR/Cas9n transfection) from the parental 832/13 β cell line and compared their function following clonal expansion. 832/13 cells were originally derived from parental INS-1 cells using a stable transfection strategy with a plasmid directing human insulin (*hINS*) expression and containing a neomycin resistance gene for antibiotic selection (Hohmeier et al., 2000). Analysis of insulin expression in cells subjected to CRISPR/Cas9n gene disruption revealed that some subclones expressed *hINS* whereas others did not (Figure S1A). We therefore reasoned that either *hINS* expression was driving functional heterogeneity or that functional heterogeneity is an inevitable product of monoclonal derivation. To address these possibilities, we reselected *hINS* expressing 832/13 cells by culture in the presence of neomycin (Figure S1B). Selected cells maintained as a polyclonal population had robust GSIS responses (Figure S1C) and the predicted enrichment of the *hINS* transcript (Figure S1D). Derivation of ten new monoclones from either the unselected 832/13 population (Figures S1E and S1F) or the neomycin-selected 832/13 population (Figures S1H and S1I) resulted in functional heterogeneity independent of *hINS* gene expression (Figures S1G and S1J, respectively). Last, we chose a newly expanded 832/13 subclone, 1327/06, and derived 20 new monoclones (1327/06a–1327/06t). Again, we found that this process resulted in widely variable GSIS responses (Figures S1K and S1L) and that these responses appeared to be normally distributed (Figure S1M). Taken together, these findings demonstrate that the clonal heterogeneity of the 832/13 cell line persists even following antibiotic selection, that normally distributed functional heterogeneity exists even when subclones are further derived from a new parental 832/13 subclone, and that caution should be exercised when using selected monoclonal cell lines for either stable transfection studies or CRISPR/Cas9 gene disruption. These findings are likely not unique to INS-1-derived cell lines and may have affected assays of SIRT3 function in other β cell lines, such as MIN-6, studied by stable transfection methods.

Stable Integration of Different SIRT3 Transgenes in Expanded SIRT3 KO Cells Yields Polyclonal Cell Lines with Concordant GSIS Responses

The foregoing observations suggested the need to develop a different *in vitro* model in which we could reliably evaluate the effects of the SIRT3-targeted acetylproteome on β cell function. Based on findings summarized in Figures S1K-S1M, we developed a strategy to

generate an *in vitro* model in a polyclonal cell line setting so that phenotypes represent the average of the normal functional distribution (Figure 1E). We reasoned that the previously generated SIRT3 KO cell lines would be maximally permissive to mitochondrial protein acetylation. Therefore, these cells would be ideal parental cell lines in which to introduce different forms of SIRT3 with or without deacetylase activity. Two expanded SIRT3 KO monoclones (SIRT3 KO 1 and SIRT3 KO 3) were used as parental cell lines in which we stably overexpressed V5-tagged human forms of either wild-type SIRT3 (hSIRT3 WT-V5), β-galactosidase (β-gal-V5), or three different enzymatically inactive forms of hSIRT3 (hSIRT3 N229A-V5, hSIRT3 H248Y-V5, and hSIRT3 NA/HY-V5) (Figure 1F; Schwer et al., 2002). These cell lines are referred to hereafter as WT, KO, NA, HY, and DM (double mutant), respectively. Following antibiotic selection, these two sets of five different polyclonal cell lines were expanded for further study.

We validated the presence of the different constructs by immunoblot analysis (Figure 1G). Only overexpression of an enzymatically active form of SIRT3 (hSIRT3 WT-V5) would be predicted to cause a decrease in mitochondrial protein acetylation in the parental SIRT3 KO cells, whereas overexpression of SIRT3 mutant gene products that lack deacetylase activity should exhibit relative mitochondrial protein hyperacetylation similar to that observed in the KO lines. Notably, SIRT3 protein was completely undetectable in KO cells, whereas the WT, NA, HY, and DM cell lines had levels of hSIRT3-V5 protein that were approximately 70-fold higher than the endogenous rSIRT3 by immunoblot analysis. As expected, analysis of GSIS revealed no significant differences among the SIRT3-null β cell lines, validating our strategy (Figures 1H–1J and 1K-1M). Surprisingly, the four SIRT3-null cell lines exhibited GSIS identical to the WT cell line (hSIRT3 WT-V5 overexpression in SIRT3 KO cells). These findings suggest that either the overexpressed hSIRT3 WT-V5 fusion protein did not deacetylate mitochondrial proteins in the parental SIRT3 KO β cells under standard culture conditions or that changes in the SIRT3-targeted acetylproteome do not influence GSIS.

SIRT3 KO β Cells with Re-expressed hSIRT3 WT-V5 Have Deacetylated Mitochondrial Proteins but No Differences in Fuel-Stimulated Insulin Secretion

SIRT3 is the predominant mitochondrial protein deacetylase (Lombard et al., 2007). To gain an initial understanding of how manipulation of SIRT3 expression affected protein acetylation in our engineered β cell lines, we prepared mitochondrial subfractions from each cell line for immunoblot analysis with a pan acetyllysine antibody following culture under three conditions: standard medium (RPMI 1640 medium, INS-1 supplement, and 10% fetal bovine serum [FBS]), confluent for 1 day; serumdeprived medium (RPMI 1640 medium, INS-1 supplement, 0.5% FBS, and 0.2% BSA), confluent for 1 day; and serumdeprived medium (RPMI 1640 medium, INS-1 supplement, 0.5% FBS, and 0.2% BSA), confluent for 6 days. As predicted (Figure 2A), we observed that, compared with KO cells, WT cells exhibited markedly less mitochondrial protein acetylation, whereas HY and KO cells had similar hyperacetylation profiles (Figure 2B). We also found that the SIRT3-null cell lines cultured at confluence in serum-deprived medium for 6 days exhibited global increases in mitochondrial protein acetylation by immunoblot relative to the other culture conditions. Increased acetylation could reasonably be attributed to the lengthened culture time over which acetyl-CoA could nonenzymatically acetylate proteins, as proposed previously

(Wagner and Payne, 2013; Weinert et al., 2015). Further, long-term culture under serum deprivation conditions can also be considered a mimetic of prolonged fasting or caloric restriction, conditions reported to cause increased mitochondrial protein acetylation (Hebert et al., 2013; Still et al., 2013; Weinert et al., 2015).

Recent work on GSIS points to important roles for extramitochondrial metabolic pathways, including glycolysis, the pentose-phosphate pathway, and cytosolic metabolism of citrate and isocitrate (Ferdaoussi et al., 2015; Gooding et al., 2015; Huang and Joseph, 2014; Spégel et al., 2013). We therefore studied pyruvate-stimulated insulin secretion (PSIS) in addition to GSIS, reasoning that pyruvate has a more direct path to mitochondrial metabolism that could unveil functional differences in our cell lines with different levels of SIRT3 activity. In β cells that were confluent for 1 day in either standard culture medium or serum-deprived medium, we found no differences in insulin secretion in response to 2.8 mM glucose (2.8 G), 1 mM pyruvate (1 P), or 16.7 mM glucose (16.7 G) (Figure 2C). In β cells that were confluent for 6 days in serum-deprived medium, the condition that yielded the greatest changes in immunoblot acetyllysine signals in the KO and HY cell lines (Figure 2B), both GSIS and insulin secretion responses to a full pyruvate dose curve (0.063–10 mM) were identical in all three cell lines (Figure 2D), with no differences in half maximal effective concentration (EC_{50}) for pyruvate (Figure 2E).

Metabolic Pathways that Impart Control over Fuel-Stimulated Insulin Secretion Are Represented in the SIRT3-Targeted β Cell Acetylproteome

To further probe the apparent discrepancies between our findings and those reported in the existing literature (Caton et al., 2013; Zhang et al., 2016; Zhou et al., 2017), we next used a large-scale mass spectrometry-based proteomics approach to identify proteins with significant differences in lysine acetylation in the β cell lines with varying levels of SIRT3 activity. We enriched mitochondria from WT, KO, and HY cell lines cultured at confluence in serum-deprived medium for 6 days and performed tandem mass tag (TMT)-based quantitative acetylproteomics (Figure 3A) using previously described methods (McDonnell et al., 2016). We identified 1,216 acetylpeptides at 1% qualitative false discovery rate (FDR), which mapped to 1,220 unique sites of acetylation on 539 proteins (representatives from parsimonious protein groups). Of the 865 acetylpeptides that contained reliable quantitative information, we further assessed 626 uniquely acetylated lysines that mapped to 242 mitochondrial proteins validated by MitoCarta 2.0 (Calvo et al., 2016; see Figure 3B for a summary and Table S1 for all acetylpeptide and protein abundance data). Compared with the KO cell line, 140 of the 626 unique lysines had a statistically significant decrease in relative acetylation abundance at quantitative 10% FDR in the WT β cell line, whereas only 1 lysine reached this degree of statistical significance in the HY cell line. We noted that multiple proteins exhibited a trend toward decreased acetylation in HY cells compared with KO cells. These changes were not statistically significant but may suggest some residual deacetylase activity in the hSIRT3 H248Y-V5 mutant. Because the one significantly deacetylated lysine in the HY cell line was also identified in the 140 significantly deacetylated lysines in the WT cell line, it was considered a false positive (well within our estimated 10% quantitative FDR). The remaining 139 sites were defined as SIRT3 targets. Overall, SIRT3 significantly deacetylated 139 (22%) of the identified acetylated lysines and,

thus, potentially affected the function of 81 (33%) of the identified acetylated mitochondrial proteins (Figure 3B). We manually cross-referenced the 81 identified proteins with the UniProt database to assign the proteins to different metabolic pathways (Figure 3C). We found changes in acetylation among proteins critical for mitochondrial energy production, including several involved in fatty acid oxidation, the TCA cycle, and the electron transport chain. Additionally, we identified proteins involved in regulation of protein quality control (PROTEIN QC) and proteins involved in detoxification of reactive oxygen species (ROS detox). Notably, although GRP78 was not detected in our analysis, we did identify K130 of SOD2 as a SIRT3 target. However, K68 of SOD2, the previously identified site of acetylation (Zhou et al., 2017), was not found in our analysis. Further breakdown of the SIRT3-targeted pathways (Figure 3C) into their individual constituent proteins illustrates the differences in relative acetylation abundance of unique lysines on specific proteins (Figures 3D–3H). In sum, our proteomics approach detected broad and significant differences in acetylation of multiple proteins in important mitochondrial pathways in cell lines engineered for different levels of SIRT3 expression and activity, but these changes had no effect on glucose- or pyruvate-stimulated insulin secretion.

Manipulation of Mitochondrial Protein Acetylation Has No Impact on the Effect of Glucose to Change Metabolite Levels in the β Cell

The lack of a SIRT3-dependent effect on glucose- or pyruvatestimulated insulin secretion suggests the possibility that the observed changes in acetylation do not affect glucose metabolism or signaling intermediates required for regulation of insulin secretion. To directly address this possibility, we performed targeted gas chromatography-mass spectrometry (GC-MS)-and mass spectrometry/mass spectrometry-based metabolic profiling on WT, KO, and HY cell lines during glucose stimulation using previously described methods (Ferrara et al., 2008; Jensen et al., 2006). Switching all three cell lines from 2.8 mM to 16.7 mM glucose and incubation for 2 hr caused robust increases in all measured TCA cycle intermediates (pyruvate, citrate, alpha-ke-toglutarate, succinate, fumarate, and malate) (Figure 4A), in agreement with previous work from our group (Jensen et al., 2006). The level of alpha-ketoglutarate (α-KG) during glucose stimulation was increased by 6.3% in WT compared with KO cells ($p = 0.045$), and malate was 11.5% and 16.1% increased in WT and HY cells, respectively, compared with KO cells ($p = 0.034$ and $p = 0.002$, respectively), but these minimal changes did not affect insulin secretion. Similarly, of 16 amino acids measured by mass spectrometry-mass spectrometry, two were robustly increased by glucose stimulation in all three cell lines (Ala and Glx, a combined measure of glutamate and glutamine), and one was decreased (Asx, a combined measure of aspartate and asparagine), with no glucose-induced changes in the other 13 amino acids, again consistent with our previous findings (Ferdaoussi et al., 2015). Ala levels measured in glucose-stimulated WT cells were 9.2% higher than in KO cells ($p = 0.033$), whereas levels of Glx in WT and HY cells were 8.8% and 9.3% greater than in KO cells, respectively ($p = 0.05$ and $p = 0.036$, respectively) (Figure 4B). In addition, measurement of 20 acylcarnitine species derived from mitochondrial metabolism of glucose, fatty acids, and amino acids revealed no differences among the cell lines in response to glucose stimulation. All three cell lines exhibited a decrease in levels of the long-chain fatty acid-derived acylcarnitines C16, C18, and C18:2 in response to glucose stimulation, consistent with glucose-dependent

production of malonyl-CoA to serve as an inhibitor of the CPT1 system, which generates long-chain acylcarnitines for β-oxidation (Figure 4C). However, despite the representation of multiple fatty acid oxidation enzymes in the SIRT3-targeted acetylproteome of the β cell (Figures 3C and 3D), no differences were found in lipid-derived acylcarnitine species among the three cell lines (Figure 4C). Overall, broad changes in mitochondrial protein acetylation in response to manipulation of SIRT3 had a minimal effect on responses of mitochondrial metabolites to glucose stimulation.

Differences in the SIRT3-Targeted Acetylproteome Do Not Affect β Cell Viability or Function in the Presence of Stress-Inducing Agents

Chronic nutrient overload is a driver of metabolic diseases and cellular stress. In obesity leading to T2D, islet β cells can be exposed to chronic hyperlipidemia and gradual elevations in blood glucose levels. A common *in vitro* model for simulating this stressful environment is culture of β cell lines or isolated islets in elevated concentrations of glucose and fatty acids, sometimes referred to as “glucolipotoxicity” (Poitout and Robertson, 2008). Several groups have reported that siRNA-mediated suppression of SIRT3 renders β cells more vulnerable to oxidative and ER stress when cultured in elevated concentrations of palmitate, whereas overexpression of SIRT3 is protective under these same conditions (Kim et al., 2015; Zhang et al., 2016; Zhou et al., 2017). A potential limitation of these prior studies was the use of siRNA-mediated knockdown for producing only partial suppression of SIRT3, allowing for residual deacetylase activity. We therefore re-visited the relationship of nutritional stress and SIRT3 with our engineered cell lines. We cultured WT, KO, and HY cells at confluence in serum-deprived medium for 6 days to achieve the remodeling of the acetylproteome defined in Figure 3 and then replaced this medium with serum-deprived medium containing 11.1 mM glucose supplemented with either 0.5 mM of a 2:1 mixture of oleate:palmitate (O/P) conjugated to BSA or BSA alone for an additional 48 hr. As expected, culture of cells under glucolipotoxic conditions caused clear impairment of insulin secretion in response to 1 mM pyruvate or 16.7 mM glucose (Figure 5A). However, there were no differences in insulin secretion among the three cell lines, suggesting that management of the SIRT3-targeted acetylproteome is not involved in mediating changes in fuel-stimulated insulin secretion under glucolipotoxic conditions.

We also investigated the effect of SIRT3 on apoptotic signaling in response to nutritional and ER stress-inducing agents. Culture of the WT, KO, and HY cell lines under glucolipotoxic conditions caused a trend to increase caspase 3 cleavage in all three cell lines that did not achieve statistical significance (Figures 5B and 5C). To test the effect of an ER stress inducer, we cultured the three cell lines at confluence in serum-deprived medium for 6 days and then replaced this medium with serum-deprived medium containing 10 nM thapsigargin (Tg) or DMSO for an additional 48 hr. Tg induced a clear increase in cleaved caspase 3 that was of similar magnitude in the three cell lines (Figures 5B and 5C). These data support the conclusion that manipulation of the SIRT3-targeted acetylproteome does not affect β cell apoptosis in response to glucolipotoxicity or ER stress.

Acylation of mitochondrial proteins is thought to occur via a nonenzymatic mechanism proportional to the matrix concentration of acyl-CoA species and time of exposure (Davies

et al., 2016; Paik et al., 1970; Weinert et al., 2013, 2014). Unique characteristics of mitochondria, including the relative alkalinity of the matrix and high concentrations of acetyl-CoA, render mitochon drial proteins particularly susceptible to nonenzymatic acetylation (Wagner and Payne, 2013). In an attempt to maximize generation of acetyl-CoA and, thus, nonenzymatic acetylation of proteins, all three cell lines were cultured at confluence in serum-deprived medium (0.5% FBS) containing 2.8 mM glucose and 10 mM pyruvate for 12 days. Immunoblot analysis confirmed significant SIRT3-dependent differences in acetylation of multiple proteins under these conditions (Figures 5D and 5E). However, both GSIS and insulin secretion in response to a broad range of pyruvate levels (0.063–10 mM) remained unchanged (Figures 5F and 5G). Thus, even under conditions of chronic substrate stress designed to maximize the modifying agent (acetyl-CoA), the presence or absence of SIRT3 had no effect on glucose- or pyruvate-stimulated insulin secretion.

Finally, we considered the possibility that the complete SIRT3 KO achieved with CRISPR/Cas9 technology caused a compensatory shift in the expression of enzymes in metabolic pathways such that acetylation-dependent phenotypes were masked in these cells. To address this, we analyzed the expression of 5,897 quantifiable proteins across our cell lines by mass spectrometry (Table S1). This analysis revealed that the expression levels of only 54 of the 5,897 proteins (0.9%) changed by ≥20%, with $p < 0.05$, in WT compared with KO cells (Figure 5H; Tables S1 and S2). Notably, we detected a strong increase in the expression of SIRT3 protein in WT compared with KO cells, serving as a positive control for our proteomics method. Pathway analysis of the 54 proteins with altered expression using the RatMine UniProt Keywords enrichment tool (Smith et al., 2012) revealed no pathway enrichment (Benjamini-Hochberg adjusted $p = 0.10$, 10% FDR). Therefore, it is highly unlikely that compensatory shifts in protein expression account for the absence of acetylation-dependent effects on β cell function in our engineered cell lines.

Effects of Global SIRT3 KO on Insulin Secretion and Glycemic Control in Mice Fed STD or HFHS Diets

Although INS-1-derived cell lines have served as a robust model for studies of β cell function in many laboratories, it remains important to test key findings from cell line studies in primary islet β cells. Global SIRT3 KO mice were created in either the 129Sv or C57BL/6J background (Hirschey et al., 2011; Lombard et al., 2007). The latter animals have a mutation in their nicotinamide nucleotide transhydrogenase (*Nnt*) gene that affects mitochondrial nicotinamide adenine dinucleotide (NAD^+):NADH and nicotinamide adenine dinucleotide phosphate ($NADP^+$):NADPH (reduced form of nicotinamide adenine dinucleotide phosphate) balance. Given the important role of NAD^+ in mitochondrial sirtuin activity and the emergent role of NADPH in regulation of GSIS, we thought that our studies would be best performed in a background of normal NNT activity. We therefore crossed global SIRT3 KO mice on the C57BL/6J, NNT-deficient background with wild-type C57BL/6NJ mice, ultimately generating a new C57BL/6J/*Nnt* wild-type SIRT3 KO line (Figures S2A and S2B).

We fed these mice either an STD diet or a diet supplemented with 45% fat and 35% carbohydrate, primarily sucrose (HFHS) for 12 weeks. At the end of the 12-week feeding period, the body weights of the HFHS diet-fed animals were significantly increased compared with the STD diet-fed animals, with no significant difference between genotypes. HFHS diet-fed mice had significant elevations in circulating glucose levels following 5 or 16 hr of fasting compared with STD diet-fed animals, again with no significant difference between genotypes. Interestingly, HFHS diet feeding resulted in significant fasting hyperinsulinemia in WT animals, with only a trend toward increased insulin levels in HFHS diet-fed SIRT3 KO animals (Table S3).

We performed immunoblot analysis of pancreatic islets pooled from SIRT3 KO and WT mice with a pan-acetyllysine antibody. These experiments revealed that islets from SIRT3 KO mice had increased protein acetylation when fed either the STD diet or the HFHS diet (Figure 6A). Additionally, islets from SIRT3 KO mice fed HFHS diet exhibited a modest trend of increased protein acetylation compared with islets from SIRT3 KO mice fed STD diet.

Glucose tolerance tests were performed to assess insulin secretion *in vivo*. In animals fed the STD diet, no genotype-specific differences were found in glucose or insulin excursions in response to oral or intraperitoneal glucose tolerance testing (oGTT and ipGTT, respectively) (Figures 6B and 6C). There were also no genotype-specific differences in insulin sensitivity as measured by an insulin tolerance test (ITT) (Figure 6D). Mice fed the HFHS diet had clear glucose intolerance and insulin resistance compared with mice fed the STD diet, but again with no genotype-specific differences (Table S3; Figures 6E–6G). However, HFHS diet feeding did reveal that SIRT3 KO mice have lower insulin levels in response to an ipGTT but not oGTT (Figures 6E and 6F), mainly because of the significant decrease in fasting insulin in these animals (Table S3). However, this impairment did not affect glycemic control during an oGTT or ipGTT (Figures 6E and 6F, respectively).

Islets from SIRT3 KO Animals Fed STD Diet Have Normal Insulin Secretion, whereas Islets from SIRT3 KO Mice Fed HFHS Diet Secrete Less Insulin in Response to a Wide Array of Secretagogues

Finally, as a direct measure of islet function in response to global SIRT3 deletion, we performed islet perifusion experiments using 60 size-matched islets isolated from individual animals from each cohort. We tested insulin secretion in response to stimulatory glucose and in the presence and absence of known potentiators of insulin secretion, including fatty acids, GLP-1, and GIP. SIRT3 KO islets from animals fed an STD diet were not significantly different from their WT controls in their insulin secretion responses to any of the tested secretagogues, with the exception of an increase in response to the depolarizing agent KCl (Figures 7A and 7B). In contrast, islets from SIRT3 KO HFHS diet-fed animals secreted significantly less insulin compared with their WT controls in response to all secretagogues studied (Figures 7C and 7D), in agreement with the reduced insulin secretion observed during the ipGTT (Figure 6F).

DISCUSSION

Previous studies have implicated the mitochondrial deacetylase SIRT3 in regulation of β cell function and survival (Caton et al., 2013; Kim et al., 2015; Zhang et al., 2016; Zhou et al., 2017). However, these studies did not include analyses of global changes in mitochondrial protein acetylation or effects on metabolism, a major mechanism through which SIRT3 is presumed to exert its biological effects (Baeza et al., 2016). The goal of our study was to fill this void and define the role of the SIRT3-targeted acetylproteome as it pertains to β cell metabolism and fuel-stimulated insulin secretion. To address these gaps in knowledge, we performed *in vitro* studies with a set of cell lines in which CRISPR/Cas9n technology (Ran et al., 2013) was used to completely eliminate endogenous SIRT3 (in contrast to previous studies, which were performed in partial siRNA or shRNA knockdown models), followed by stable overexpression of active or inactive forms of the enzyme. Key findings of the *in vitro* studies were as follows. Manipulation of SIRT3 expression results in clear changes in acetylation of a broad group of mitochondrial enzymes involved in fatty acid oxidation, the TCA cycle, the electron transport chain, and other pathways. These differences had negligible effects on glucose-induced changes in an array of metabolites measured by GC-mass spectrometry and mass spectrometry-mass spectrometry. Glucose-and pyruvate-stimulated insulin secretion responses were identical across the full panel of engineered cell lines despite significant differences in mitochondrial protein acetylation. Global differences in the SIRT3-targeted acetylproteome did not affect responses to β cell stress-inducing agents.

In addition, studies in our global SIRT3 KO, C57BL/6J/ *Nnt* wild-type mouse model revealed the following. Acetylation of multiple proteins was increased in islets obtained from SIRT3 KO compared with WT mice in both the STD diet and HFHS diet settings. When fed the STD diet, SIRT3 KO mice given an oral or intraperitoneal (i.p.) glucose load exhibited glucose excursions and insulin secretion responses indistinguishable from those of WT mice. When fed the HFHS diet, a nutritional stress that caused clear glucose intolerance in both genotypes, SIRT3 KO and WT mice had identical glucose excursions following either an oral or i.p. glucose load. Despite the identical glucose tolerance curves, insulin levels were lower in SIRT3 KO mice compared with WT mice during the ipGTT but not the oGTT. Perifusion studies with islets isolated from both the STD dietand HFHS diet-fed cohorts corroborated the *in vivo* findings. Thus, there were no significant differences in insulin secretion in islets from SIRT3 KO compared with WT mice fed the STD diet, except for a modest increase in the response to the general depolarizing agent KCl in islets from SIRT3 KO mice. In contrast, islets from SIRT3 KO mice fed the HFHS diet had smaller secretion responses to all secretagogues and potentiators studied, including glucose, fatty acids, GLP-1, GIP, and KCl, relative to islets from WT mice fed the HFHS diet.

Our findings contrast in some respects with those in the literature. For example, partial suppression of SIRT3 in the INS-1 or NIT-1 β cell lines via siRNA transfection reportedly resulted in increased ROS production and markers of ER stress, decreased cell viability, activation of apoptosis, impaired insulin secretion, and exacerbated palmitate-induced dysfunction (Caton et al., 2013; Zhang et al., 2016). In another study, stable expression of a SIRT3-specific shRNA in the MIN-6 β cell line decreased glucose-stimulated ATP content,

impaired GSIS, and also increased susceptibility to palmitate-induced dysfunction (Zhou et al., 2017). In related studies, overexpression of SIRT3 by plasmid transfection or adenoviral transduction protected insulinoma cells against palmitate-induced dysfunction (Kim et al., 2015; Zhang et al., 2016; Zhou et al., 2017). However, these studies did not report the effects of SIRT3 manipulation on intermediary metabolism. Moreover, with the exception of GRP78 (Zhang et al., 2016) and SOD2 (Zhou et al., 2017), the extent to which partial siRNA-or shRNA-mediated suppression of SIRT3 expression altered the mitochondrial acetylproteome was not investigated. In our own studies with partial siRNA-mediated suppression of SIRT3 in the 832/13 cell line, we found little, if any, change in mitochondrial protein acetylation, as measured by anti-pan acetyllysine immunoblotting, suggesting that incomplete and transient SIRT3 knockdown may not be a reliable approach for assessing the role of protein acetylation in islet cell function. Also, the specificity of the siRNA and shRNA constructs used in the prior studies was not detailed, opening the possibility that the reported changes in β cell function could have been due to off-target effects. In addition, the changes in function reported in previous work using stably expressed shRNA constructs (Zhou et al., 2017) could have been driven by clonal variability, as we encountered in the current work and overcame by genetic engineering in polyclonal cell populations. Finally, we also considered the possibility that the complete SIRT3 KO afforded by the CRISPR/Cas9 technology might have induced compensatory changes in protein expression to offset effects of hyperacetylation. However, analysis of the expression levels of more than 5,800 proteins by mass spectrometry-based proteomics revealed very small protein expression changes in the WT cell line compared with the KO cell line. We conclude that the current study, in which we engineered a broad range of SIRT3 activity levels coupled with large-scale acetylproteomics, protein expression proteomics, and targeted metabolomics analyses, provides an in-depth assessment of the effect of SIRT3 on β cell function and stress responses. The main conclusion from our *in vitro* studies is that SIRT3 activity clearly modifies the acetylproteome but has no discernable effect on mitochondrial metabolism, fuel-stimulated insulin secretion, or responses to a variety of stressors, including elevated lipids and apoptosis-inducing agents.

We note that our β cell lines exhibit a broad dynamic range in which to study the effect of SIRT3 expression; although the KO β cell line expresses no detectable endogenous rSIRT3, the WT line express ~70-fold more hSIRT3 WT-V5 compared with endogenous rSIRT3 protein in the parental cell line. Thus, in theory, mitochondrial proteins in KO cells should be maximally hyperacetylated, whereas mitochondrial proteins in WT cells should be maximally deacetylated. However, even when these cell lines were cultured under conditions to maximally induce acetylation (e.g., 12 days of culture in serum-deprived and pyruvate-supplemented medium), SIRT3-dependent changes in mitochondrial protein acetylation had no effect on fuel-stimulated insulin secretion.

Quantitative acetylproteomics revealed significant differences in acetylation of several components of multiple metabolic pathways critical for mitochondrial energy production, including fatty acid oxidation, the TCA cycle, and the electron transport chain. The most affected proteins in the fatty acid oxidation pathway were subunits A and B of the mitochondrial trifunctional enzyme (3-hydroxyacyl-coenzyme dehydrogenase A [HADHA] and HADHB), which accounted for 17 of this pathway's 32 SIRT3-targeted lysines.

Interestingly, our proteomics analysis also found changes in acetylation of short-chain HADH, the enzyme responsible for the penultimate step in β-oxidation of fatty acids, which has been ascribed a role in insulin secretion. Patients with genetic deficiencies in *HADH* exhibit hyperinsulinemia (Clayton et al., 2001), and siRNA-mediated suppression of HADH in both 832/13 β cells and mouse islets results in increased basal insulin secretion (Hardy et al., 2007). However, despite significant differences in acetylation of multiple HADH lysines, we found no evidence of increased insulin secretion at basal glucose (2.8 mM) across the three cell lines in multiple experiments. Further, the intracellular concentrations of a broad swath of acylcarnitine species derived from fatty acid oxidation were indistinguishable across the WT, KO, and HY cell lines, suggesting that mitochondrial lipid metabolism was not perturbed. Several enzymes in the TCA cycle also exhibited differences in acetylation between the WT and KO cell lines. These included proteins previously reported to be inhibited by acetylation, such as pyruvate dehydrogenase (PDHA1) (Jing et al., 2011), mitochondrial $NADP^+$- dependent isocitrate dehydrogenase (IDH2) (Someya et al., 2010), subunit A of the succinate dehydrogenase complex (SDHA) (Finley et al., 2011), and mitochondrial malate dehydrogenase (MDH2) (specifically, acetylation of K239) (Hebert et al., 2013). However, differences in acetylation of these and other TCA cycle components did not appreciably affect glucoseinduced changes in organic acids, amino acids, or acylcarnitines, suggesting that glucose metabolism was largely unchanged. With the exception of complex III, we found differences in acetylation of at least one subunit of each of the electron transport chain complexes (I–V) as well as the ADP:ATP ratio translocase 1 (SLC25A4). Notably, acetylation has been reported to inhibit NADH dehydrogenase and ATP synthase, whereas deacetylation by SIRT3 restores their activities and ATP production (Ahn et al., 2008; Bao et al., 2010). Our acetylproteomics analysis indicated that acetylation of multiple lysines of an accessory subunit of NADH dehydrogenase (NDUFV3) and acetylation of multiple subunits of ATP synthase (ATP5C1, ATP5F1, ATP5H, ATP5J, and ATP5O) are significantly different between the WT and KO cell lines. However, these changes in acetylation did not influence fuel-stimulated insulin secretion or metabolism. Given that a rise in the ATP:ADP ratio is an important stimulus-secretion coupling factor for GSIS (Muoio and Newgard, 2008), this suggests that electron transport chain function remains largely intact despite significant differences in acetylation of multiple electron transport chain complex proteins in response to manipulation of SIRT3 expression.

To examine the role of mitochondrial protein acetylation in the primary β cell in the presence and absence of nutritional stress, we also studied global SIRT3 KO mice. Prior studies of SIRT3 ablation in mice have suggested its involvement in the regulation of systemic metabolism and susceptibility to diet-induced metabolic dysregulation (Dittenhafer-Reed et al., 2015; Hirschey et al., 2011; Jing et al., 2011; Lantier et al., 2015; Zhou et al., 2017). Several of those studies have been performed in the 129Sv mouse strain background. We chose to study whole-body deletion of SIRT3 in the C57BL/6 strain, given its more rapid and robust development of diet-induced obesity and metabolic dysfunction. When our study was initiated, the SIRT3 KO mice were in a C57BL/6J background, which harbors a mutation in the gene that encodes mitochondrial nicotinamide nucleotide transhydrogenase (*Nnt*) (Hirschey et al., 2011; Lombard et al., 2007). Mitochondrial NNT catalyzes trans-hydrogenation between NADH and $NADP^+$. The end products, NAD^+

(necessary for SIRT3 activity) and NADPH (involved in GSIS) could, in theory, increase the dynamic range of protein acetylation and islet function phenotypes observed in SIRT3 KO and WT mice. In fact, comparison of *Nnt* wild-type and *Nnt* mutant mice reveals a defect in insulin secretion in the latter strain (Fergusson et al., 2014). Therefore, we bred the wild-type form of *Nnt* back into the C57BL/6J animals with global deletion of SIRT3. We selected an HFHS Western diet (45% kilocalories [kcal] from fat and 35% kcal from carbohydrates, primarily sucrose) as the dietary stress because of its potential to drive carbon stress via multiple macronutrients. As expected, we were able to detect hyperacetylation of multiple proteins in SIRT3 KO islets compared with WT islets following 12 weeks of either STD diet or HFHS diet feeding. Notably, we did not observe a diet-dependent decrease in SIRT3 expression in these pooled islets from WT mice, unlike what has been reported in other rodent models in both islet and non-islet tissues (Hirschey et al., 2011; Lantier et al., 2015; Zhang et al., 2016; Zhou et al., 2017).

With STD diet-feeding, SIRT3 KO mice were similar in weight to WT controls and exhibited identical fasting plasma glucose and insulin levels. Glucose excursion in response to either an oral or i.p. glucose bolus was indistinguishable between genotypes, in contrast to two other studies, in which whole-body deletion of SIRT3 was reported to result in significant glucose intolerance, even in animals fed STD diet (Hirschey et al., 2011; Jing et al., 2011). In our study, SIRT3 KO and WT mice fed the STD diet also had identical insulin secretion responses to either an oral or i.p. glucose load. These findings demonstrate that, in the absence of nutritional stress, increased acetylation of pancreatic islet proteins permitted by the absence of SIRT3 is not sufficient to affect glycemic control or insulin secretion. These findings are consistent with the results from our cell line studies.

HFHS diet feeding resulted in marked obesity and significant increases in fasting blood glucose compared with STD diet-feeding in both the SIRT3 KO and WT backgrounds. Fasting plasma insulin levels were significantly lower in the SIRT3 KO compared with WT mice fed the HFHS diet. Glucose tolerance, measured either as oGTT or ipGTT, was markedly impaired by the HFHS diet compared with STD diet feeding but was not different in HFHS diet-fed SIRT3 KO and WT mice. This contrasts with prior studies that reported glucose intolerance in SIRT3 KO mice on a 129Sv background in response to HFD feeding (Hirschey et al., 2011; Zhou et al., 2017). Notably, the feeding period was considerably longer in the Hirschey et al. (2011) study (~55 weeks) compared with the current study (12 weeks). Insulin secretion in response to the oGTT was not significantly different in SIRT3 KO compared with WT mice. In contrast, insulin levels were lower in response to ipGTT in the SIRT3 KO mice. Identical i.p. glucose excursions in the two genotypes, occurring in the face of a smaller insulin response in the SIRT3 KO strain, could have suggested that peripheral insulin sensitivity was enhanced in the SIRT3 KO mice, but an insulin tolerance test did not reveal a significant difference in insulin sensitivity.

The foregoing insulin secretion phenotypes were largely corroborated in perifusion studies of islets isolated from the STD diet- and HFHS diet-fed groups of mice. Here we were able to control for islet number and size to facilitate the comparison of genotypes. Insulin secretion from islets isolated from STD diet-fed SIRT3 KO mice was not different from that observed with islets from STD diet-fed wild-type controls for all secretagogues tested, with

the exception of a statistically significant increase in response to a depolarizing concentration of KCI. Interestingly, islets from HFHS diet-fed SIRT3 KO mice secreted less insulin in response to all secretagogues and potentiators studied relative to islets from HFHS diet-fed wild-type mice, including KCI. The impairment in GSIS is similar to that reported previously in islets from HFD-fed SIRT3 KO animals measured in a static incubation assay (Zhou et al., 2017). Although the mechanisms underlying reduced insulin secretion in HFHS diet-fed animals remain unknown, we think that it is unlikely to be occurring via a β cell-intrinsic mechanism. We base this in part on our findings of equal impairment of insulin secretion in response to exposure of insulinoma cells engineered for absent or high SIRT3 expression to glucolipotoxic conditions, an *in vitro* mimetic of nutritional stress such as induced by HFHS diet feeding *in vivo* (Poitout and Robertson, 2008). These findings suggest, instead, that the reduction in insulin secretion observed in islets from HFHS diet-fed mice occurs as a consequence of interaction of islets lacking SIRT3 with factors produced in peripheral tissues that are specific to the HFHS diet-fed SIRT3 KO background. Identification of these putative factors is a topic for future investigation.

Other nutritional conditions have been reported to increase protein acetylation, notably fasting or caloric restriction, conditions that activate mobilization of fatty acids and generation of acetyl-CoA via fatty acid oxidation (Hebert et al., 2013; Still et al., 2013; Weinert et al., 2015). Although we did not study chronically fasted animals, we did simulate a form of caloric restriction in studies shown in Figures 2 and 5. In Figure 2, we serum-deprived the WT, HY, and KO cell lines by culture in 0.5% FBS for 6 days. This protocol brought out a much larger increase in protein acetylation in KO or HY cells versus WT cells, as measured by immunoblot (Figure 2B), than observed in the same cells cultured for 1 day in medium containing 0.5% FBS or the normal supplement of 10% FBS. Despite this, there were no differences in glucose- or pyruvate-stimulated insulin secretion in SIRT3-null cell lines compared with the WT cell line subjected to the 6 days of serum deprivation (Figure 2D). Similarly, as shown in Figure 5, culture of the various cell lines under serum-deprived conditions for 12 days in the presence of low glucose (2.8 mM) and a high pyruvate load (10 mM) to drive production of acetyl-CoA yielded the expected relative hyperacetylation in the KO and HY lines relative to the WT (Figures 5D and 5E), but again with no effect on glucose-or pyruvate-stimulated insulin secretion (Figures 5F and 5G). These data suggest that it is unlikely that metabolic changes occurred as a function of combined serum deprivation plus SIRT3 KO.

In sum, we find that broad changes in mitochondrial protein acetylation occurring as a function of manipulation of SIRT3 expression are not sufficient to causes changes in islet function. In fact, dramatic remodeling of the mitochondrial acetylproteome in β cell lines via exaggerated manipulation of SIRT3 expression has no discernable effect on insulin secretion, mitochondrial metabolism, or responses to external stress-inducing agents. Similarly, global KO of SIRT3 in mice fed STD diet has negligible effects on insulin secretion despite clear effects on protein acetylation. Only when global SIRT3 KO animals are subjected to chronic nutrient stress via HFHS diet feeding do genotype-specific differences in insulin secretion emerge. It remains to be determined whether the modest trend of increased protein acetylation observed in islets from HFHS diet-fed versus STD diet-fed SIRT3 KO mice (Figure 6A) contributes to impairment of islet cell metabolism or

function. A full understanding of this issue requires an assessment of the stoichiometry of lysine acetylation on specific proteins, which was not possible with the proteomics methods used here. In this regard, recent estimates of the stoichiometry of lysine acetylation suggest that only a small percentage of the specific protein molecules in a cell are acetylated on specific lysines, even under conditions of SIRT3 ablation (Weinert et al., 2015). Given that the anti-pan acetyllysine antibody used in Figure 6A detects only a subset of the most abundant acetylated proteins, more robust changes in acetylation of less abundant proteins could be occurring. However, even if this is the case, the change in insulin secretion observed in HFHS diet-fed SIRT3 KO animals is not sufficient to alter glucose homeostasis during oGTT or ipGTT, suggesting that any such changes in acetylation stoichiometry have limited physiological or pathophysiological significance.

STAR★METHODS

Detailed methods are provided in the online version of this paper and include the following:

CONTACT FOR REAGENT AND RESOURCE SHARING

Further information and requests for resources and reagents should be directed to and will be fulfilled by the Lead Contact, Christopher Newgard, PhD (chris.newgard@duke.edu).

EXPERIMENTAL MODEL DETAILS

Cell Culture Studies

The INS-1-derived 832/13 rat insulinoma cell line was cultured as previously described (Hohmeier et al., 2000) unless otherwise indicated. For experiments using conditioned cell culture media: 1) Serum-deprived media was defined as RPMI-1640 with 11.1 mM glucose supplemented with 0.5% fetal bovine serum (FBS), 0.2% bovine serum albumin (BSA) (SIGMA #A7979), 10 mM HEPES, 2 mM glutamine, 1 mM sodium pyruvate, and 50 uM β-mercaptoethanol; 2) High-pyruvate media was defined as RPMI-1640 without glucose supplemented with 2.8 mM glucose, 0.5% FBS, 0.2% BSA, 10 mM HEPES, 2 mM glutamine, 10 mM sodium pyruvate, 50 uM β-mercaptoethanol, and 8.3 mM mannitol; 3) Glucolipotoxicity-inducing media was defined as RPMI-1640 with 11.1 mM glucose supplemented with 0.5 mM of 2:1 oleate:palmitate mixture conjugated to fatty acid-free BSA (O/P) (SIGMA #A9576), 0.5% fetal bovine serum (FBS), 0.2% bovine serum albumin (BSA), 10 mM HEPES, 2 mM glutamine, 1 mM sodium pyruvate, and 50 uM β-mercaptoethanol; 4) ER stress-inducing media was defined as RPMI-1640 with 11.1 mM glucose supplemented with 10 nM Thapsigargin, 0.5% fetal bovine serum (FBS), 0.2% bovine serum albumin (BSA), 10 mM HEPES, 2 mM glutamine, 1 mM sodium pyruvate, and 50 uM β-mercaptoethanol. All reagents and solutions were obtained from Sigma-Aldrich unless otherwise indicated.

Animal Studies

SIRT3 KO mice on a 129Sv background were a kind gift from Professor Eric Verdin, Buck Institute. They were rederived upon arrival at Duke University in the C57BL/6J strain (JAX Stock No: 000664) and continually backcrossed onto this background for greater than 10

generations to generate C57BL/6J SIRT3 mice. These mice were then crossed with the C57BL/6NJ strain (JAX Stock No: 005304) until homozygous for wild-type NNT, to generate breeders for the C57BL/6J/*Nnt* wild-type SIRT3 KO line used in this study. At 11-14 weeks of age, male mice were fed either a standard diet (Lab Diet #5053) or a high-fat/high-sucrose diet (Research Diets #D12451) for 12 weeks. For glucose-tolerance tests, mice were fasted for 5 hr before administering 1.5 mg/g body weight of glucose via oral gavage (oGTT) or intraperitoneal injection (ipGTT). Blood glucose was measured from tail vein blood at 0, 10, 20, 30, 60, 90, and 120 min post-bolus. Tail vein blood was collected at 0, 10, and 30 min post-bolus for plasma insulin measurements. For insulin tolerance tests (ITT), mice were fasted for 5 hr before administering 0.5 mU/g body weight Humalog (Eli Lilly) via intraperitoneal injection. Blood glucose was measured at 0, 10, 20, 30, 60, and 90 min post-injection. Blood glucose was measured with a Bayer Contour glucometer. Plasma insulin was assayed using the STELLUX Chemi Rodent Insulin ELISA (ALPCO). All animal protocols were approved by the Institutional Animals Use and Care Committee at Duke University.

METHOD DETAILS

CRISPR/Cas9n

For the generation of SIRT3 KO β-cell lines: 1) pSpCas9n(BB)-2A-Puro (PX462) was a kind gift from Feng Zhang (Addgene plasmid #48141); 2) Oligonucleotide guide RNA (gRNA) sequences directed at the SIRT3 gene were designed using the Massachusetts Institute of Technology's "Optimized CRISPR Design" web tool (found online at http://crispr.mit.edu/), and purchased from Integrated DNA Technologies (IDT). Briefly, the paired gRNA targeting sequences used to generate SIRT3 KO 1 and SIRT3 KO 2 cell lines were 5'-ACATTGGGCCTGTAGTGCCC-3' and 5'-CCTTCGGCTGCTTCACGACA-3', while the paired gRNA targeting sequences for SIRT3 KO 3 and SIRT3 KO 4 cell lines were 5'-GCTTCAACCAGCTTTGAGGC-3' and 5'-CTACGTGCACGGTCTGTCGA-3'. gRNA targeting sequences were annealed to complimentary RNA oligonucleotides and subsequently ligated into separate BbsI-digested PX462 vector backbones for a total of four (two pairs) of plasmids. Plasmids were transformed and amplified in Subcloning Efficiency DH5α Competent Cells (Thermo #18265017) and purified using QIAprep Spin Miniprep Kit (QIAGEN #27104). 832/13 cells were cotransfected with either pair of SIRT3-targeting plasmids or an equal mass of empty vector as a control using TransIT-LT1 (Mirus Bio #2300) reagent according to manufacturer's instructions. Transfection media was replaced with full media 18 hr following transfection for an additional 24 hr of resistance marker expression. Full media was replaced with full media supplemented with 1.5 ug/mL Puromycin for selection and was refreshed every 24 hr for 48-96 hr. Selected cells were suspended and plated at a limiting dilution in full media. Newly isolated monoclones were expanded and screened for SIRT3 protein expression by immunoblot with a SIRT3-specific antibody (Cell Signaling Technology #5490).

Lentiviral Constructs and Lentivirus

For the generation of lentiviral constructs: 1) The wild-type human SIRT3 (hSIRT3 WT) fusion protein open reading frame flanked by attR1 and attR2 sites was synthesized as a

gBlock Gene Fragment from IDT; 2) The Gateway pDONR221 Vector (Thermo #12536017) was used according to manufacturer's instructions; 3) The pLenti6.3/V5-DEST Gateway Vector Kit (Thermo #V53306) was used according to manufacturer's instructions. Briefly, the hSIRT3 WT gBlock Gene Fragment was cloned into the pDONR221 vector according to manufacturer's instructions to generate the pDONR221/hSIRT3 WT plasmid. Using the pDONR221/hSIRT3 WT plasmid as a template, the QuikChange Lightning Multi Site-Directed Mutagenesis Kit (Agilent #210513) was used according to manufacturer's instructions to generate pDON221/hSIRT3 N229A, pDON221/hSIRT3 H248Y, and double mutant pDON221/hSIRT3 NA/HY sequence-verified plasmids. pDONR221/hSIRT3 plasmids were recombined with pLenti6.3/V5-DEST vector to generate sequence-verified pLenti6.3/hSIRT3-V5 plasmids according to manufacturer's instructions. Lentivirus was produced by transfecting either pLenti6.3/V5-GW/lacZ or one of the five different pLenti6.3/hSIRT3-V5 plasmids into HEK293T cells using the ViraPower Lentiviral Packaging Mix (Thermo #K497500) according to manufacturer's instructions. SIRT3 KO 1 and SIRT3 KO 3 β-cell lines were infected with the different lentiviruses in a confluent 25 cm^2 cell culture flask. Lentiviral media was replaced with full media 24 hr following infection for an additional 24 hr of resistance marker expression. Full media was replaced with full media supplemented with 2 ug/mL Blasticidin for selection and was refreshed every 48 hr until no death was observed. The two sets of five different stably infected polyclonal mixtures of β-cells were carried forward for study.

Cell Fractionation and Immunoblot Analysis

Mitochondrial enrichments: Confluent cells from a 175 cm^2 flask were washed with ice-cold PBS, lifted in 0.05% trypsin-EDTA, resuspended in ice-cold PBS supplemented with 10% FBS and 10 mM NAM, and pelleted at 750 ×g in a4°C. Cells were washed once more in ice-cold PBS supplemented with 10 mM NAM and pelleted. The pellet was resuspended in 1 mL of ice-cold MSH buffer (220 mM mannitol, 70 mM sucrose, 5 mM HEPES, 10 mM NAM) and homogenized with 50 strokes in a Dounce homogenizer on ice. Following a 5 min 750 × g centrifugation at 4°C, the supernatant was aliquoted in a separate tube and kept on ice. The remaining pellet was re-suspended in 500 μL ice-cold MSH buffer and homogenized; the above steps were repeated twice more. Pooled supernatants were pelleted at 15,000 ×g in a 4°C centrifuge and re-suspended in 500 ×L ice-cold MSH for two subsequent wash steps. The pelleted mitochondria-enriched fraction was lysed in 30 ×L of MSH buffer supplemented with 0.1% Triton X-100 and the Halt Protease Inhibitor Cocktail (Thermo #78430).

To prepare insulinoma and primary islet cell lysates, cells/tissue were lysed in ice-cold RIPA buffer with Halt Protease Inhibitor Cocktail (Thermo #78430). Clarified lysates were resolved on 4%–12% NuPAGE gels (Invitrogen) and transferred to nitrocellulose membranes (Bio-Rad). The membranes were first stained with Ponceau S for total protein images in the colorimetric channel of a Gel Doc imager (Bio-Rad). Ponceau S was thoroughly washed with TBS-T (TBS containing 0.1% Tween 20) prior to blocking membrane with 5% milk in TBS-T. Following wash steps, membranes with resolved proteins were probed with the following primary antibodies: Anti-SIRT3 (Cell Signaling Technology #2627), anti-Total OXPHOS Cocktail (abcam #ab110413), anti-V5Tag (Thermo

#MA5-15253), anti-Citrate Synthase (Origene #TA308265), anti-Acetylated-Lysine (Cell Signaling Technology #9441), anti-UQCRSF1 (Abcam #14746), anti-β-actin (Cell Signaling Technology #8457), and anti-Caspase 3 (Cell Signaling Technology #9662). Primary antibodies were detected with the following secondary antibodies: Donkey anti-rabbit IRDye 800CW (Li-COR #926-32213) and donkey antimouse IRDye 680RD (Li-COR #926-68072). Immunoblots were developed and quantified using an Odyssey CLx system (Li-COR).

RNA Isolation and qPCR Analysis

RNA was isolated from cells using the QIAGEN RNeasy Mini Kit (QIAGEN) and reverse transcribed with the iScript cDNA Synthesis Kit (Bio-Rad) according to manufacturer's instructions. Real-time quantitative PCR (qPCR) analysis was performed using iTaq Universal SYBR Green Supermix (Bio-Rad) and indicated primer sequences (Table S4). Human *INS* (*hINS*) gene expression was measured using TaqMan Gene Expression Assay Hs00355773_m1 (Thermo #4331182). qPCR assays were run using the ViiA 7 Real-Time PCR System (Thermo). See Table S4 for qPCR primer sequence information.

Fuel-Stimulated Insulin Secretion

For glucose- and pyruvate-stimulated insulin secretion experiments, collectively referred to as fuel-stimulated insulin secretion (FSIS), cells were seeded in 24-well plates (Corning) and cultured to confluence unless otherwise stated. Cells were pre-incubated in a HEPES balanced salt solution (HBSS) secretion buffer (114 mM NaCl, 4.7 mM KCl. 1.2 mM KH_2PO_4, 1.16 mM $MgSO_4$, 20 mM HEPES, 2.5 mM $CaCl_2$, 25.5 mM $NaHCO_3$, 0.2% BSA, pH 7.2) containing 2.8 mM glucose for 2 hr. Following pre-incubation, cells were stimulated for 2 hr in secretion buffer containing either 2.8 mM glucose, 16.7 mM glucose, or 2.8 mM glucose supplemented with a range of sodium pyruvate concentrations (0.063 mM -10 mM). Secretion buffer was sampled at the end of the experiment, diluted as necessary, and assayed using the STELLUX Chemi rodent insulin ELISA kit (ALPCO). Cells were lysed in ice-cold RIPA buffer with Halt Protease Inhibitor Cocktail (Thermo #78430) and clarified lysates were assayed for total cellular protein using the BCA Protein Assay Kit (Thermo #23225). FSIS data are represented as insulin secreted per total cellular protein per hour.

Acetylproteomics

Sample preparation

Mitochondrial pellets were re-suspended in 300 μL of ice-cold 8M Urea Lysis Buffer (8 M urea in 50mM Tris, pH 8.0, 40 mM NaCl, 2 mM $MgCl_2$, 1× complete mini EDTA-free protease inhibitor tablet, 10 mM Nicotinamide, 10 μM TSA). The mitochondria were disrupted by a combination of pipetting and vortexing, and subsequent sonication with a probe sonicator in three 5 s bursts (power setting of 3), incubating on ice between each burst. Samples were centrifuged at 10,000 × g for 10 min at 4°C and the supernatant was retained. Protein concentration was determined by BCA, and equal amount of protein (500 μg, adjusted to 2.5 mg/mL with Urea Lysis Buffer) from each sample was reduced with 5 mM DTT at 37°C for 30 min, cooled to RT, alkylated with 15 mM iodoacetamide for 30 min in the dark and unreacted iodoacetamide quenched by the addition of DTT up to 15 mM. Each

sample was digested with 5 μg LysC (100:1 w/w, protein to enzyme) at 37°C for 4 hr. Following dilution to 1.5 M urea with 50 mM Tris (pH 8.0), 5 mM $CaCl_2$, the samples were digested with trypsin (50:1 w/w, protein:enzyme) overnight at 32°C. The samples were acidified to 0.5% trifluoroacetic acid (TFA) and centrifuged at 4,000 μ g for 10 min at 4°C to pellet insoluble material. The supernatant was desalted by solid phase extraction (SPE) with a Waters 50 mg tC18 SEP-PAK SPE column and the eluate was frozen and dried in a speed vac. Each sample was resuspended in 100 μL of 200 mM triethylammonium bicarbonate (TEAB), mixed with a unique 10-plex Tandem Mass Tag (TMT) reagent (0.8 μg re-suspended in 50 μL 100% acetonitrile), and shaken for 5 hr at room temperature. After samples were quenched with 0.8 μL 50% hydroxylamine and shaken for 15 additional min at RT, all nine samples were combined, frozen, and dried in a speed vac. The mixture was re-suspended in 1 mL 0.5% TFA and subjected to SPE with a Waters 100 mg tC18 SEP-PAK SPE column. The eluate was vortexed and split into aliquots containing ~5% of the total peptide mixture (250 μg) and a second aliquot containing ~95% (4.75 mg). Both aliquots were frozen and dried in a speed vac. The 250 μg aliquot of the “input” material was saved at −80°C for quantification of unmodified peptides.

Acetylpeptide enrichment and input fractionation

The 4.75 mg aliquot was re-suspended in 1.4 mL 1X IAP Buffer and subjected to immunoprecipitation (IP) with PTMScan Acetyl Lysine Motif IAP Beads on a rotator overnight at 4°C. The next day, the antibody-peptide complexes were pelleted via centrifugation at 2,000 × g for 30 s and the precipitate was washed 2 times in 1 mL of IP buffer and 3 times in 1 mL water (centrifuging each time). Acetylpeptides were eluted twice with 100 ×L of 0.15% TFA for 10 min each time, and the supernatants from each elution were combined, acidified to 0.5% TFA (and brought to a 1 mL volume), desalted on a 50 mg tC18 SEP-PAK SPE column, frozen, and dried in a speed vac. The “input” material was separated into 8 fractions using a High pH Reversed Phase Peptide Fractionation Kit (Pierce #84868). After column conditioning, 100 μg of peptide re-suspended in 300 μL 0.1% TFA was loaded onto a fractionation column and centrifuged at 3,000 × g for 2 min at RT. Sample was washed with 300 μL water followed by 300 μL of 5% acetonitrile (ACN), 0.1% TFA. Sample was eluted in 8 fractions containing increasing amount of ACN, frozen, and dried in a speed vac. Peptide fractions were re-suspended in 10 μL of 0.1% formic acid (FA) and quantified using the Quantitative Colorimetric Peptide Assay (Pierce, 23275).

Nano-LC-MS/MS

All samples were subjected to *nano*LC-MS/MS analysis using an EASY-nLC UPLC system (Thermo Fisher Scientific) coupled to a *Q Exactive Plus* Hybrid Quadrupole-Orbitrap mass spectrometer (Thermo Fischer Scientific) via an EASY-Spray (Thermo Fischer Scientific) nanoelectrospray ionization source. Prior to injection, the acetylpeptide sample was re-suspended in 22.5 μL 1% FA and each of the HPRP fractions of the input material were re-suspended in enough 0.1% FA to achieve a peptide concentration of approximately 0.15 μg/μL (which was determined precisely using the peptide quantitation assay described above). The acetylpeptide sample was analyzed with technical triplicate runs, with 6.5 μL of sample injected for each. The 8 input HPRP fractions were analyzed in singlicate, with 1 ug injections (roughly 7 μL for each based on the precise concentration). For each injection, the

sample was first trapped on an Acclaim PepMap 100 C18 trapping column (3 μm particle size, 75 μm × 20 mm) with 18 μL of solvent A (0.1% FA) at a variable flow rate dictated by max pressure of 500 Bar, after which the analytical separation was performed over a 105 min gradient (flow rate of 300 nL/minute) of 5 to 40% solvent B (90% ACN, 0.1% FA) using an Acclaim PepMap RSLC C18 analytical column (2 um particle size, 75 μm × 500 mm column (Thermo Fischer Scientific) with a column temperature of 55°C. MS^1 (precursor ions) was performed at 70,000 resolution, with an AGC target of 3×10^6 ions and a maximum injection time of 60 ms. MS^2 spectra (product ions) were collected by data-dependent acquisition (DDA) of the top 10 most abundant precursor ions with a charge greater than 1 per MS1 scan, with dynamic exclusion enabled for a window of 30 s. Precursor ions were filtered with a 0.7 m/z isolation window and fragmented with a normalized collision energy of 30. MS2 scans were performed at 35,000 resolution, with an AGC target of 1×10^5 ions and a maximum injection time of 60 ms.

Raw data processing

Raw LC-MS/MS data have been deposited to the ProteomeXchange Consortium via the PRIDE partner repository (Vizcaíno et al., 2016) with the dataset identifier PXD009509. Raw LC-MS/MS data were processed in Proteome Discoverer v2.2 (PD2.2, Thermo Fisher Scientific), using both the Sequest HT (Yates, 2015) and MS Amanda 2.0 (Dorfer et al., 2014) search engines. Data were searched against the UniProt rat (*Rattus norvegicus*) complete proteome database of reviewed (Swiss-Prot) and unreviewed (TrEMBL) proteins, which consisted of 29,979 sequences on the date of download (9/20/2017). Default search parameters included oxidation (15.995 Da on M) as a variable modification and carbamidomethyl (57.021 Da on C) and TMT (229.163 Da on peptide N-term and K). To assess labeling efficiency as a quality control measure, the input fraction was re-searched with N-terminal TMT as a variable modification, confirming N-terminal labeling of 91% of all PSMs. Acetylpeptide runs added acetyl (42.01057 Da on K) as a variable modification and changed TMT to a variable modification on K (remaining fixed on peptide N-term). Data were searched with a 10 ppm precursor mass and 0.02 Da product ion tolerance. The maximum number of missed cleavages was set to a default value of 2 (but changed to 4 for acetyl runs) and enzyme specificity was trypsin (full). Considering each data type (acetyl, input) separately, peptide spectral matches (PSMs) from each search algorithm were filtered to a 1% false discovery rate (FDR) using the Percolator (Käll et al., 2007) node of PD2.2. For acetyl data, site localization probabilities were determined for acetyl lysines using the ptmRS algorithm (Tausetal., 2011). PSMs were grouped to unique peptides while maintaining a 1% FDR at the peptide level and using a 90% site localization threshold for acetyl lysines. Peptides from all samples (acetyl, input) were grouped to proteins together using the rules of strict parsimony and proteins were filtered to 1% FDR using the Protein FDR Validator node of PD2.2. Reporter ion intensities for all PSMs having co-isolation interference below 50% (of the ion current in the isolation window) and average reporter S/N > 2.5 were summed together at the peptide group and protein level, but keeping quantification for each data type (acetyl, input) separate. Peptides shared between protein groups were excluded from protein quantitation calculations.

Statistical analysis

Protein and peptide groups tabs in the PD2.2 results were exported as tab delimited .txt. files, opened in Microsoft EXCEL, and analyzed as described previously (McDonnell et al., 2016). First, peptide group reporter intensities for each peptide group in the input material were summed together for each TMT channel, each channel's sum was divided by the average of all channels' sums, resulting in channel-specific loading control normalization factors to correct for any deviation from equal protein/peptide input into the nine-sample comparison. Reporter intensities for peptide groups from the acetyl fraction and for proteins from the input fraction were divided by the loading control normalization factors for each respective TMT channel. Analyzing the acetylpeptide and protein datasets separately, all loading control-normalized TMT reporter intensities were converted to log2 space, and the average value from the nine samples was subtracted from each sample-specific measurement to normalize the relative measurements to the mean. For each cell line (WT, KO, HY), condition average and standard deviation were calculated. For each comparison (WT/HY, WT/KO, HY/KO), Log2 fold change, p value (two-tailed Student's t test, assuming equal variance), and adjusted p value ($P_{adjusted}$, Benjamini Hochberg FDR correction) were calculated (Benjamini et al., 2001; Lesack and Naugler, 2011). For protein-level quantification, only Master Proteins—or the most statistically significant protein representing a group of parsimonious proteins containing common peptides identified at 1% FDR—were used for quantitative comparison. Acetylpeptide measurements were calculated both alone (referred to as "relative abundance") and with normalization to any change in the corresponding Master Protein (referred to as "normalized acetylation ratio"), calculated by subtracting Log2 Master Protein values from acetylpeptide quantitation values on a sample-specific basis (See Table S1 for all acetylpeptide and protein abundance data).

Metabolite Profiling

Cells were seeded in 21 cm^2 cell culture dishes (Greiner). Organic acids, amino acids, and acylcarnitines were analyzed using a stable isotope dilution technique. Organic acids were quantified using methods described previously (Jensen et al., 2006) employing a Trace Ultra GC coupled to a ISQ MS operating under Xcalibur 2.2 (Thermo Fisher Scientific, Austin, TX). Amino acids and acylcarnitine measurements were made by flow injection tandem mass spectrometry using sample preparation methods described previously (An et al., 2004; Ferrara et al., 2008). These data were acquired using a Waters TQD mass spectrometer equipped with a Acquity UPLC system and controlled by the MassLynx 4.1 operating system (Waters, Milford, MA).

Islet Isolation and Perifusion

Primary islets were isolated from mice as previously described (Lamont et al., 2012). 60 size-matched islets were handpicked into 0.275 mL chambers containing KRBPH (135 mM NaCl, 3.6 mM KCI, 1.5 mM $CaCl_2$, 0.5 mM NaH_2PO_4, 0.5 mM $MgSO_4$, 5 mM HEPES, 5 mM $NaCO_3$, 1% BSA, pH 7.4). Islets were perifused for 48 min of equilibration in KRBPH with 2.8 mM glucose at a flow rate of 200 µl per min using the Biorep Perifusion system. Following equilibration, islets were perifused at a flow rate of 200 µL per min with KRBPH supplemented with the following secretagogues/potentiators for the following times: 1) 2.8

mM glucose for 8 min; 2) 16.7 mM glucose for 16 min; 3) 2.8 mM glucose for 16 min; 4) 11.1 mM glucose for 12 min; 5) 11.1 mM glucose with 0.5 mM O/P for 12 min; 6) 11.1 mM glucose for 12 min; 7) 11.1 mM glucose with 0.03 nM GLP-1 for 12 min; 8) 11.1 mM glucose for 12 min; 9) 11.1 mM glucose with 0.3 nM GIP for 12 min; 10) 11.1 mM glucose for 12 min; 11) 2.8 mM glucose for 12 min; and 12) 2.8 mM glucose with 30 mM KCl for 12 min. Perifusion media was collected at 1 min-intervals for measurement of insulin concentrations. Insulin was detected with the AlphaLISA Biomarker Detection Kit (PerkinElmer) and insulin concentrations were determined using the EnVision 2105 Multimode Plate Reader (PerkinElmer). Data are represented as ng insulin secreted per mL of buffer.

QUANTIFICATION AND STATISTICAL ANALYSIS

Analysis for all studies was performed using GraphPad Prism6 unless otherwise stated. Data are presented as the mean ± SE unless otherwise stated. Data were analyzed busing a Two-Way ANOVA with Bonferroni post hoc corrections for multiple comparisons or the two-tailed unpaired, Student's t test unless otherwise stated.

DATA AND SOFTWARE AVAILABILITY

The accession number for the raw LC-MS/MS proteomics data reported in this paper is ProteomeXchange Consortium via the PRIDE partner repository (Vizcaino et al., 2016) PRIDE: PXD009509 (see Key Resources Table). Table S1 contains the full proteomics datasets.

Supplementary Material

Refer to Web version on PubMed Central for supplementary material.

ACKNOWLEDGMENTS

The authors would like to thank Eoin McDonnell and Jon Haldeman for assistance with cloning of CRISPR/Cas9 and viral constructs; Lisa Poppe for assistance with cell culture; and Jingjing Niu, Sara Encisco, and Megan Capozzi for assistance with islet perifusion experiments. We also thank Drs. Deborah Muoio, Donald McDonnell, and David D'Alessio for helpful discussion. These studies were supported by NIH grants R24 DK085610 (to C.B.N. and M.D.H.) and RO1 DK46492 and PO1 DK58398 (to C.B.N.).

REFERENCES

Ahn BH , Kim HS , Song S , Lee IH , Liu J , Vassilopoulos A , Deng CX , and Finkel, T (2008). A role for the mitochondrial deacetylase Sirt3 in regulating energy homeostasis. Proc. Natl. Acad. Sci. USA 105, 14447–14452. [PubMed: 18794531]

An J , Muoio DM , Shiota M , Fujimoto Y , Cline GW , Shulman GI , Koves TR , Stevens R , Millington D , and Newgard CB (2004). Hepatic expression of malonyl-CoA decarboxylase reverses muscle, liver and whole-animal insulin resistance. Nat. Med 10, 268–274. [PubMed: 14770177]

Baeza J , Smallegan MJ , and Denu JM (2016). Mechanisms and Dynamics of Protein Acetylation in Mitochondria. Trends Biochem. Sci 41, 231–244. [PubMed: 26822488]

Bao J , Scott I , Lu Z , Pang L , Dimond CC , Gius D , and Sack MN (2010). SIRT3 is regulated by nutrient excess and modulates hepatic susceptibility to lipotoxicity. Free Radic. Biol. Med 49, 1230–1237. [PubMed: 20647045]

Benjamini Y , Drai D , Elmer G , Kafkafi N , and Golani I (2001). Controlling the false discovery rate in behavior genetics research. Behav. Brain Res 125, 279–284. [PubMed: 11682119]

Calvo SE , Clauser KR , and Mootha VK (2016). MitoCarta2.0: an updated inventory of mammalian mitochondrial proteins. Nucleic Acids Res 44 (D1), D1251–D1257. [PubMed: 26450961]

Caton PW , Richardson SJ , Kieswich J , Bugliani M , Holland ML , Mar-chetti P , Morgan NG , Yaqoob MM , Holness MJ , and Sugden MC (2013). Sirtuin 3 regulates mouse pancreatic beta cell function and is suppressed in pancreatic islets isolated from human type 2 diabetic patients. Diabetologia 56, 1068–1077. [PubMed: 23397292]

Clayton PT , Eaton S , Aynsley-Green A , Edginton M , Hussain K , Krywa-wych S , Datta V , Malingre HE , Berger R , and van den Berg IE (2001). Hyperinsulinism in short-chain L-3-hydroxyacyl-CoA dehydrogenase deficiency reveals the importance of beta-oxidation in insulin secretion. J. Clin. Invest 108, 457–65. [PubMed: 11489939]

Davies MN , Kjalarsdottir L , Thompson JW , Dubois LG , Stevens RD ., Ilkayeva OR , Brosnan MJ , Rolph TP , Grimsrud PA , and Muoio DM (2016). The Acetyl Group Buffering Action of Carnitine Acetyltransferase Offsets Macronutrient-Induced Lysine Acetylation of Mitochondrial Proteins. Cell Rep 14, 243–254. [PubMed: 26748706]

Dittenhafer-Reed KE , Richards AL , Fan J , Smallegan MJ , Fotuhi Siah-pirani A , Kemmerer ZA , Prolla TA , Roy S , Coon JJ , and Denu JM (2015). SIRT3 mediates multi-tissue coupling for metabolic fuel switching. Cell Metab 21, 637–646. [PubMed: 25863253]

Dorfer V , Pichler P , Stranzl T , Stadlmann J , Taus T , Winkler S , and Mechtler K (2014). MS Amanda, a universal identification algorithm optimized for high accuracy tandem mass spectra. J. Proteome Res 13, 3679–3684. [PubMed: 24909410]

Ferdaoussi M , Dai X , Jensen MV , Wang R , Peterson BS , Huang C , Ilkayeva O , Smith N , Miller N , Hajmrle C , et al. (2015). Isocitrate-to-SENP1 signaling amplifies insulin secretion and rescues dysfunctional β cells. J. Clin. Invest 125, 3847–3860. [PubMed: 26389676]

Fergusson G , Ethier M , Guévremont M , Chrétien C , Attané C , Joly E , Fioramonti X , Prentki M , Poitout V , and Alquier T (2014). Defective insulin secretory response to intravenous glucose in C57Bl/6J compared to C57Bl/6N mice. Mol. Metab 3, 848–854. [PubMed: 25506550]

Ferrara CT , Wang P , Neto EC , Stevens RD , Bain JR , Wenner BR , Ilkayeva OR , Keller MP , Blasiole DA , Kendziorski C , et al. (2008). Genetic networks of liver metabolism revealed by integration of metabolic and transcriptional profiling. PLoS Genet 4, e1000034. [PubMed: 18369453]

Finley LW , Haas W , Desquiret-Dumas V , Wallace DC , Procaccio V , Gygi SP , and Haigis MC (2011). Succinate dehydrogenase is a direct target of sirtuin 3 deacetylase activity. PLoS ONE 6, e23295. [PubMed: 21858060]

Gooding JR , Jensen MV , Dai X , Wenner BR , Lu D , Arumugam R , Ferdaoussi M , MacDonald PE , and Newgard CB (2015). Adenylosuccinate is an insulin secretagogue derived from glucose-induced purine metabolism. Cell Rep 13, 157–167. [PubMed: 26411681]

Hardy OT , Hohmeier HE , Becker TC , Manduchi E , Doliba NM , Gupta RK , White P , Stoeckert CJ , Matschinsky FM , Newgard CB , and Kaestner KH (2007). Functional genomics of the beta-cell: short-chain 3-hy-droxyacyl-coenzyme A dehydrogenase regulates insulin secretion independent of K+ currents. Mol. Endocrinol 21, 765–773. [PubMed: 17185391]

Hebert AS , Dittenhafer-Reed KE , Yu W , Bailey DJ , Selen ES , Boersma MD , Carson JJ , Tonelli M , Balloon AJ , Higbee AJ , et al. (2013). Calorie restriction and SIRT3 trigger global reprogramming of the mitochondrial protein acetylome. Mol. Cell 49, 186–199. [PubMed: 23201123]

Hirschey MD , Shimazu T , Jing E , Grueter CA , Collins AM , Aouizerat B , Stančáková A , Goetzman E , Lam MM , Schwer B , et al. (2011). SIRT3 deficiency and mitochondrial protein hyperacetylation accelerate the development of the metabolic syndrome. Mol. Cell 44, 177–190. [PubMed: 21856199]

Hohmeier HE , Mulder H , Chen G , Henkel-Rieger R , Prentki M , and Newgard CB (2000). Isolation of INS-1-derived cell lines with robust ATP-sensitive K+ channel-dependent and -independent glucose-stimulated insulin secretion. Diabetes 49, 424–430. [PubMed: 10868964]

Huang M , and Joseph JW (2014). Assessment of the metabolic pathways associated with glucose-stimulated biphasic insulin secretion. Endocrinology 155, 1653–1666. [PubMed: 24564396]

Jensen MV , Joseph JW , Ilkayeva O , Burgess S , Lu D , Ronnebaum SM , Odegaard M , Becker TC , Sherry AD , and Newgard CB (2006). Compensatory responses to pyruvate carboxylase suppression in islet beta-cells. Preservation of glucose-stimulated insulin secretion. J. Biol. Chem 281, 22342–22351. [PubMed: 16740637]

Jensen MV , Joseph JW , Ronnebaum SM , Burgess SC , Sherry AD , and Newgard CB (2008). Metabolic cycling in control of glucose-stimulated insulin secretion. Am. J. Physiol. Endocrinol. Metab 295, E1287–E1297. [PubMed: 18728221]

Jensen MV , Gooding JR , Ferdaoussi M , Dai XQ , Peterson BS , Mac-Donald PE , and Newgard CB (2017). Metabolomics applied to islet nutrient sensing mechanisms. Diabetes Obes. Metab 19 (Suppl 1), 90–94. [PubMed: 28880482]

Jing E , Emanuelli B , Hirschey MD , Boucher J , Lee KY , Lombard D , Verdin EM , and Kahn CR (2011). Sirtuin-3 (Sirt3) regulates skeletal muscle metabolism and insulin signaling via altered mitochondrial oxidation and reactive oxygen species production. Proc. Natl. Acad. Sci. USA 108, 14608–14613. [PubMed: 21873205]

Käll L , Canterbury JD , Weston J , Noble WS , and MacCoss MJ (2007). Semi-supervised learning for peptide identification from shotgun proteomics datasets. Nat. Methods 4, 923–925. [PubMed: 17952086]

Kendrick AA , Choudhury M , Rahman SM , McCurdy CE , Friederich M , Van Hove JL , Watson PA , Birdsey N , Bao J , Gius D , et al. (2011). Fatty liver is associated with reduced SIRT3 activity and mitochondrial protein hyperacetylation. Biochem. J 433, 505–514. [PubMed: 21044047]

Kim M , Lee JS , Oh JE , Nan J , Lee H , Jung HS , Chung SS , and Park KS (2015). SIRT3 Overexpression Attenuates Palmitate-Induced Pancreatic β-Cell Dysfunction. PLoS ONE 10, e0124744. [PubMed: 25915406]

Lamont BJ , Li Y , Kwan E , Brown TJ , Gaisano H , and Drucker DJ (2012). Pancreatic GLP-1 receptor activation is sufficient for incretin control of glucose metabolism in mice. J. Clin. Invest 122, 388–402. [PubMed: 22182839]

Lantier L , Williams AS , Williams IM , Yang KK , Bracy DP , Goelzer M , James FD , Gius D , and Wasserman DH (2015). SIRT3 Is Crucial for Maintaining Skeletal Muscle Insulin Action and Protects Against Severe Insulin Resistance in High-Fat-Fed Mice. Diabetes 64, 3081–3092. [PubMed: 25948682]

Lesack K , and Naugler C (2011). An open-source software program for performing Bonferroni and related corrections for multiple comparisons. J. Pathol. Inform 2, 52. [PubMed: 22276243]

Lombard DB , Alt FW , Cheng HL , Bunkenborg J , Streeper RS , Mosto-slavsky R , Kim J , Yancopoulos G , Valenzuela D , Murphy A , et al. (2007). Mammalian Sir2 homolog SIRT3 regulates global mitochondrial lysine acetylation. Mol. Cell. Biol 27, 8807–8814. [PubMed: 17923681]

McDonnell E , Crown SB , Fox DB , Kitir B , Ilkayeva OR , Olsen CA , Grimsrud PA , and Hirschey MD (2016). Lipids Reprogram Metabolism to Become a Major Carbon Source for Histone Acetylation. Cell Rep 17, 1463–1472. [PubMed: 27806287]

Mulder H (2017). Transcribing β-cell mitochondria in health and disease. Mol. Metab 6, 1040–1051. [PubMed: 28951827]

Muoio DM , and Newgard CB (2008). Mechanisms of disease:Molecular and metabolic mechanisms of insulin resistance and beta-cell failure in type 2 diabetes. Nat. Rev. Mol. Cell Biol 9, 193–205. [PubMed: 18200017]

Paik WK , Pearson D , Lee HW , and Kim S (1970). Nonenzymatic acetylation of histones with acetyl-CoA. Biochim. Biophys. Acta 213, 513–522. [PubMed: 5534125]

Poitout V , and Robertson RP (2008). Glucolipotoxicity: fuel excess and beta-cell dysfunction. Endocr. Rev 29, 351–366. [PubMed: 18048763]

Prentki M , Matschinsky FM , and Madiraju SR (2013). Metabolic signaling in fuel-induced insulin secretion. Cell Metab 18, 162–185. [PubMed: 23791483]

Ran FA , Hsu PD , Lin CY , Gootenberg JS , Konermann S , Trevino AE , Scott DA , Inoue A , Matoba S , Zhang Y , and Zhang F (2013). Double nicking by RNA-guided CRISPR Cas9 for enhanced genome editing specificity. Cell 154, 1380–1389. [PubMed: 23992846]

Rardin MJ , Newman JC , Held JM , Cusack MP , Sorensen DJ , Li B , Schilling B , Mooney SD , Kahn CR , Verdin E , and Gibson BW (2013). Label-free quantitative proteomics of the lysine acetylome in mitochondria identifies substrates of SIRT3 in metabolic pathways. Proc. Natl. Acad. Sci. USA 110, 6601–6606. [PubMed: 23576753]

Schwer B , North BJ , Frye RA , Ott M , and Verdin E (2002). The human silent information regulator(Sir)2 homologue hSIRT3isamitochondrial nicotinamide adenine dinucleotide-dependent deacetylase. J. Cell Biol 158, 647–657. [PubMed: 12186850]

Smith RN , Aleksic J , Butano D , Carr A , Contrino S , Hu F , Lyne M , Lyne R , Kalderimis A , Rutherford K , et al. (2012). InterMine: a flexible data warehouse system for the integration and analysis of heterogeneous biological data. Bioinformatics 28, 3163–3165. [PubMed: 23023984]

Sol EM , Wagner SA , Weinert BT , Kumar A , Kim HS , Deng CX , and Choudhary C (2012). Proteomic investigations of lysine acetylation identify diverse substrates of mitochondrial deacetylase sirt3. PLoS ONE 7, e50545. [PubMed: 23236377]

Someya S , Yu W , Hallows WC , Xu J , Vann JM , Leeuwenburgh C , Ta-nokura M , Denu JM , and Prolla TA (2010). Sirt3 mediates reduction of oxidative damage and prevention ofage-related hearing loss under caloric restriction. Cell 143, 802–812. [PubMed: 21094524]

Spégel P , Sharoyko VV , Goehring I , Danielsson AP , Malmgren S , Nagorny CL , Andersson LE , Koeck T , Sharp GW , Straub SG , et al. (2013). Time-resolved metabolomics analysis of β-cells implicates the pentose phosphate pathway in the control ofinsulin release. Biochem. J 450,595–605. [PubMed: 23282133]

Still AJ , Floyd BJ , Hebert AS , Bingman CA , Carson JJ , Gunderson DR , Dolan BK , Grimsrud PA , Dittenhafer-Reed KE , Stapleton DS , et al. (2013). Quantification of mitochondrial acetylation dynamics highlights prominent sites of metabolic regulation. J. Biol. Chem 288, 26209–26219. [PubMed: 23864654]

Taus T , Köcher T , Pichler P , Paschke C , Schmidt A , Henrich C , and Mechtler K (2011). Universal and confident phosphorylation site localization using phosphoRS. J. Proteome Res 10, 5354–5362. [PubMed: 22073976]

Vetere A , Choudhary A , Burns SM , and Wagner BK (2014). Targeting the pancreatic β-cell to treat diabetes. Nat. Rev. Drug Discov 13, 278–289. [PubMed: 24525781]

Vizcaíno JA , Csordas A , Del-Toro N , Dianes JA , Griss J , Lavidas I , Mayer G , Perez-Riverol Y , Reisinger F , Ternent T , et al. (2016). 2016 update of the PRIDE database and its related tools. Nucleic Acids Res 44, 11033. [PubMed: 27683222]

Wagner GR , and Hirschey MD (2014). Nonenzymatic protein acylation as a carbon stress regulated by sirtuin deacylases. Mol. Cell 54, 5–16. [PubMed: 24725594]

Wagner GR , and Payne RM (2013). Widespread and enzyme-independent Nε-acetylation and Nε-succinylation of proteins in the chemical conditions of the mitochondrial matrix. J. Biol. Chem 288, 29036–29045. [PubMed: 23946487]

Weinert BT , Schölz C , Wagner SA , Iesmantavicius V , Su D , Daniel JA , and Choudhary C (2013). Lysine succinylation is a frequently occurring modification in prokaryotes and eukaryotes and extensively overlaps with acetylation. Cell Rep 4, 842–851. [PubMed: 23954790]

Weinert BT , Iesmantavicius V , Moustafa T , Schölz C , Wagner SA , Magnes C , Zechner R , and Choudhary C (2014). Acetylation dynamics and stoichiometry in Saccharomyces cerevisiae. Mol. Syst. Biol 10, 716. [PubMed: 24489116]

Weinert BT , Moustafa T , Iesmantavicius V , Zechner R , and Choudhary C (2015). Analysis of acetylation stoichiometry suggests that SIRT3 repairs nonenzymatic acetylation lesions. EMBO J 34, 2620–2632. [PubMed: 26358839]

Yates JR . (2015). Pivotal role of computers and software in mass spectrometry -SEQUEST and 20 years of tandem MS database searching. J. Am. Soc. Mass Spectrom. 26, 1804–1813. [PubMed: 26286455]

Zhang HH , Ma XJ , Wu LN , Zhao YY , Zhang PY , Zhang YH , Shao MW , Liu F , Li F , and Qin GJ (2016). Sirtuin-3 (SIRT3) protects pancreatic β-cells from endoplasmic reticulum (ER) stress-induced apoptosis and dysfunction. Mol. Cell. Biochem 420, 95–106. [PubMed: 27449933]

Zhou Y , Chung ACK , Fan R , Lee HM , Xu G , Tomlinson B , Chan JCN , and Kong APS (2017). Sirt3 Deficiency Increased the Vulnerability of Pancreatic Beta Cells to Oxidative Stress-Induced Dysfunction. Antioxid. Redox Signal 27, 962–976. [PubMed: 28375738]

Highlights

- CRISPR/Cas9 used to create β cell lines with absent or robust expression of SIRT3
- Manipulation of SIRT3 in β cells remodels the mitochondrial acetylproteome
- β cell SIRT3 does not affect insulin secretion, metabolomic profile, or survival
- SIRT3 KO only affects insulin secretion in mice fed a high-fat and high-sucrose diet

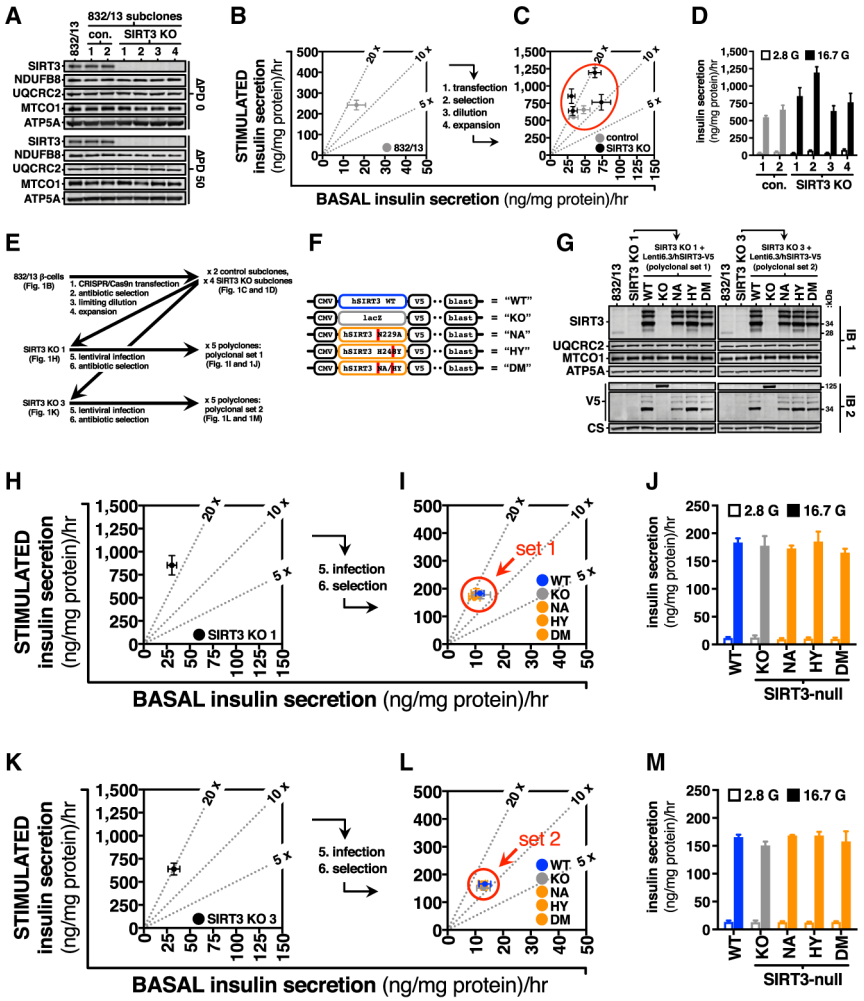

Figure 1. Stable Integration of Different SIRT3 Transgenes in SIRT3 KO Insulinoma Cells

(A) Immunoblot detection of SIRT3 and mitochondrial markers (NDUFB8, UQCRC2, MTCO1, and ATP5A) at initial point of freeze-down (ΔPD 0) and following 50 passage doublings (ΔPD 50). (B and C) GSIS performed in 832/13 cells (B) and 832/13 subclones (C). x axis (BASAL insulin secretion): insulin secretion in response to 2.8 mM glucose. y axis (STIMULATED insulin secretion): insulin secretion in response to 16.7 mM glucose. 5×, 10×, and 20× mark 5-, 10-, and 20-fold GSIS, respectively (dotted gray lines). Individual points represent one cell line. n = 4 independent experiments.

(D) GSIS; conventional presentation of data from Figure 1C.

(E) Outline of the experimental strategy used to engineer stable cell lines.

(F) Diagram of the different lentiviral constructs used to infect SIRT3 KO cells and the corresponding names of the resulting polyclonal cell lines.

(G) Immunoblot detection of the different overexpress hSIRT3-V5 fusion proteins and mitochondrial markers (UQCRC2, MTCO1, ATP5A, and CS) in 832/13 parental β cells, SIRT3 KO subclones, and two different polyclonal sets of transgenic cell lines: WT, re-expression of hSIRT3 WT-V5 in the SIRT3 KO line; KO, expression of β-gal-V5 in the SIRT3 KO line; NA, re-expression of the catalytically inactive hSIRT3 N229A-V5 mutant in

the SIRT3 KO line; HY, re-expression of the catalytically inactive hSIRT3 H248Y-V5 mutant in the SIRT3 KO line; and DM, re-expression of the catalytically inactive hSIRT3 NA/HY-V5 double mutant in the SIRT3 KO line. (H, I, K, and L) GSIS performed in SIRT3 KO 1 cells (H), polyclone set 1 (I), SIRT3 KO 3 cells (K), and polyclone set 2 (L). x axis (BASAL insulin secretion): insulin secretion in response to 2.8 mM glucose. y axis (STIMULATED insulin secretion): insulin secretion in response to 16.7 mM glucose. n = 3 independent experiments. Individual points represent one cell line. (J and M) GSIS performed in polyclone set 1 (J) and polyclone set 2 (M); conventional presentation of data from (I) and (L), respectively. Data are mean ± SE. Statistical comparisons were made using two-way ANOVA with Bonferroni's multiple comparisons test.

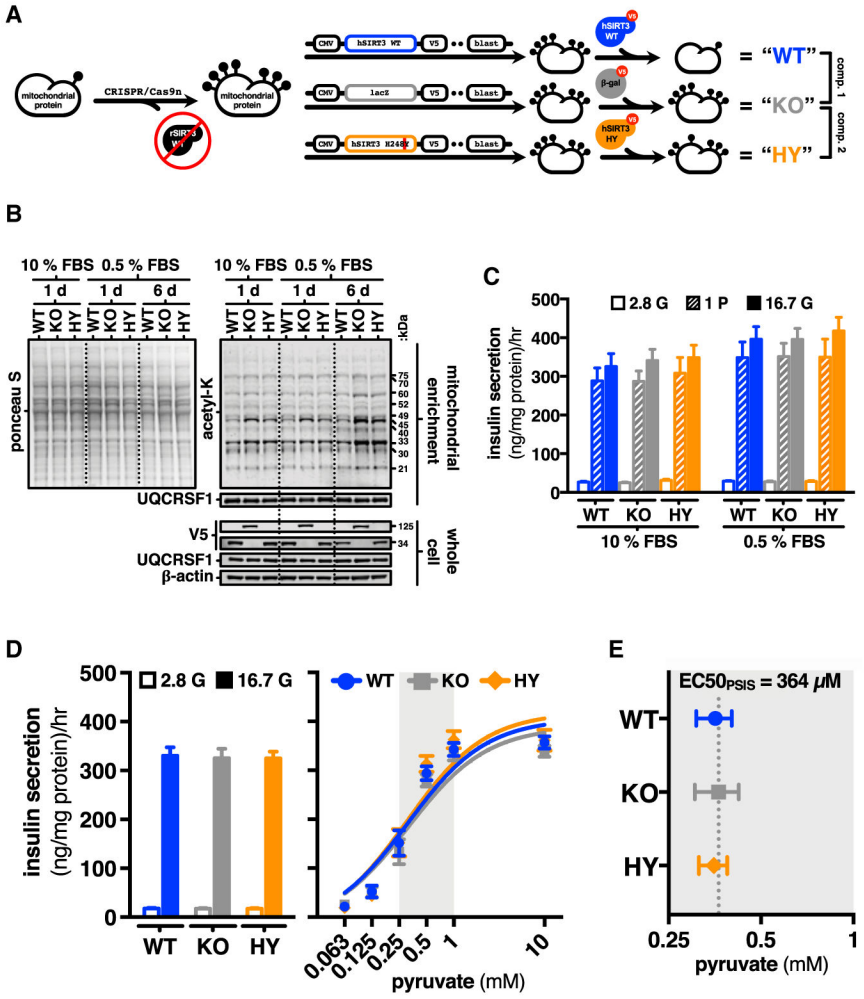

Figure 2. Differences in Mitochondrial Protein Acetylation Are Not Associated with Differences in Insulin Secretion

(A) Summary of comparisons and predicted differences in mitochondrial protein acetylation among the transgenic cell lines used in this study.

(B) Immunoblot detection of lysine acetylation (acetyl-K) in mitochondrial fractions. Cells were cultured at confluence for 1 day in either full medium or serum-deprived medium or for 6 days in serum-deprived medium. Cells were harvested and split for preparation of the mitochondrial or whole-cell samples. Black dotted lines are visual aids to help identify the culture condition groups.

(C) Fuel-stimulated insulin secretion in response to 2.8 mM glucose (2.8 G), 2.8 mM glucose supplemented with 1 mM pyruvate (1 P), or 16.7 mM glucose (16.7 G) following culture at confluence for 1 day under the respective culture conditions. n = 3 independent experiments. (D) Insulin secretion following 6 days of culture at confluence in serum-deprived medium. Left: insulin secretion in response to 2.8 and 16.7 mM glucose. Right: pyruvate-stimulated insulin secretion in response to 2.8 mM glucose supplemented with an array of pyruvate doses (63 μM–10 mM pyruvate). Dose-response curves are nonlinear fit (agonist) versus response.

(E) EC_{50} of PSIS curves in (D). n = 3 independent experiments. Data represent means ± SE. Statistical comparisons were made using two-way ANOVA with Bonferroni's multiple comparisons test.

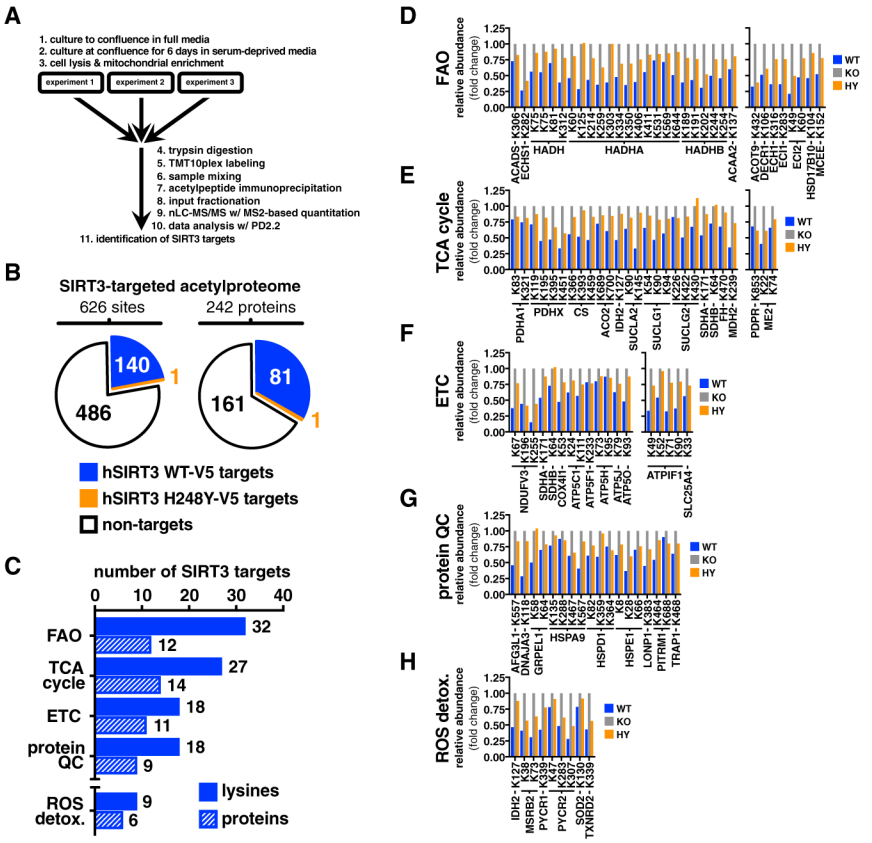

Figure 3. Significant Differences in Acetylation of the SIRT3-Targeted β Cell Acetylproteome Are Present in Pathways Involved in Glucose, Pyruvate, and Fatty Acid Metabolism

(A) Outline of the experimental strategy used to generate acetylproteomics data.

(B) Summary of results and mass spectrometrybased analysis of the SIRT3-targeted acetylproteome. Left: summary of the 626 quantifiable acetyllysines and their significant deacetylation by hSIRT3 WT-V5 and hSIRT3 H248Y-V5. Right: summary of the 242 corresponding proteins targeted for deacetylation by hSIRT3 WT-V5 and hSIRT3 H248Y-V5.

(C) Number of SIRT3-targeted lysines and protein subunits represented in manually identified pathways: fatty acid oxidation (FAO), the tricarboxylic acid (TCA) cycle, the electron transport chain (ETC), protein quality control (PROTEIN QC), and reactive oxygen species detoxification (ROS detox). (D–H) Acetylation abundance of SIRT3-targeted lysines on subunits from proteins involved in fatty acid oxidation (D), the TCA cycle (E), the electron transport chain (F), protein quality control (G), and ROS detoxification (H). Data are represented as acetylpeptide abundance relative to lysines in KO cells set to 1. n = 3 independently prepped mitochondrial fractions.

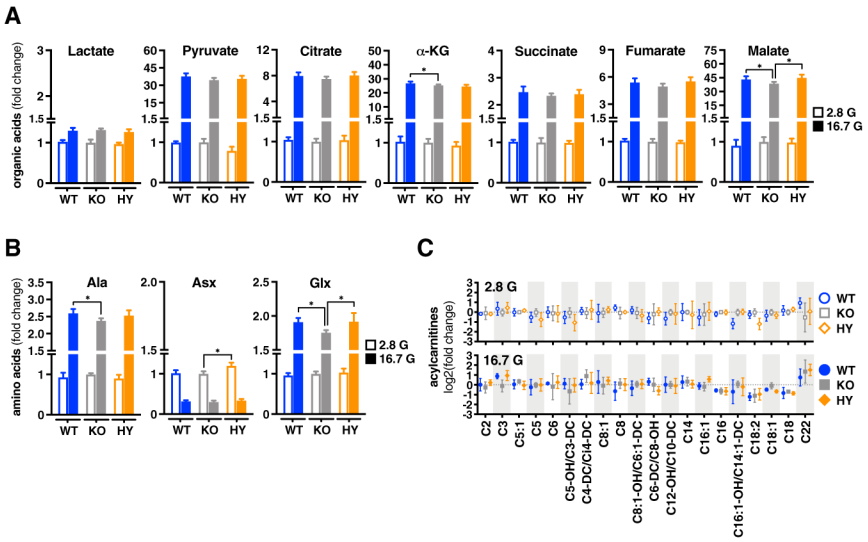

Figure 4. Glucose-Stimulated Changes in Intracellular Metabolites Are Unaffected by Changes in the SIRT3-Targeted β Cell Acetylproteome

(A and B) Fold changes of intracellular (A) organic acids and (B) amino acids in response to stimulation with 2.8 or 16.7 mM glucose. (C) Log2 fold changes of intracellular acylcarnitines in cells exposed to 2.8 or 16.7 mM glucose. Fold change values were normalized to KO cells treated with 2.8 mM glucose set to 1. n = 4 replicates. Data are represented as mean ± SE. Statistical comparisons were made using twoway ANOVA with Bonferroni's multiple comparisons test. *p ≤ 0.05 effect of cell line.

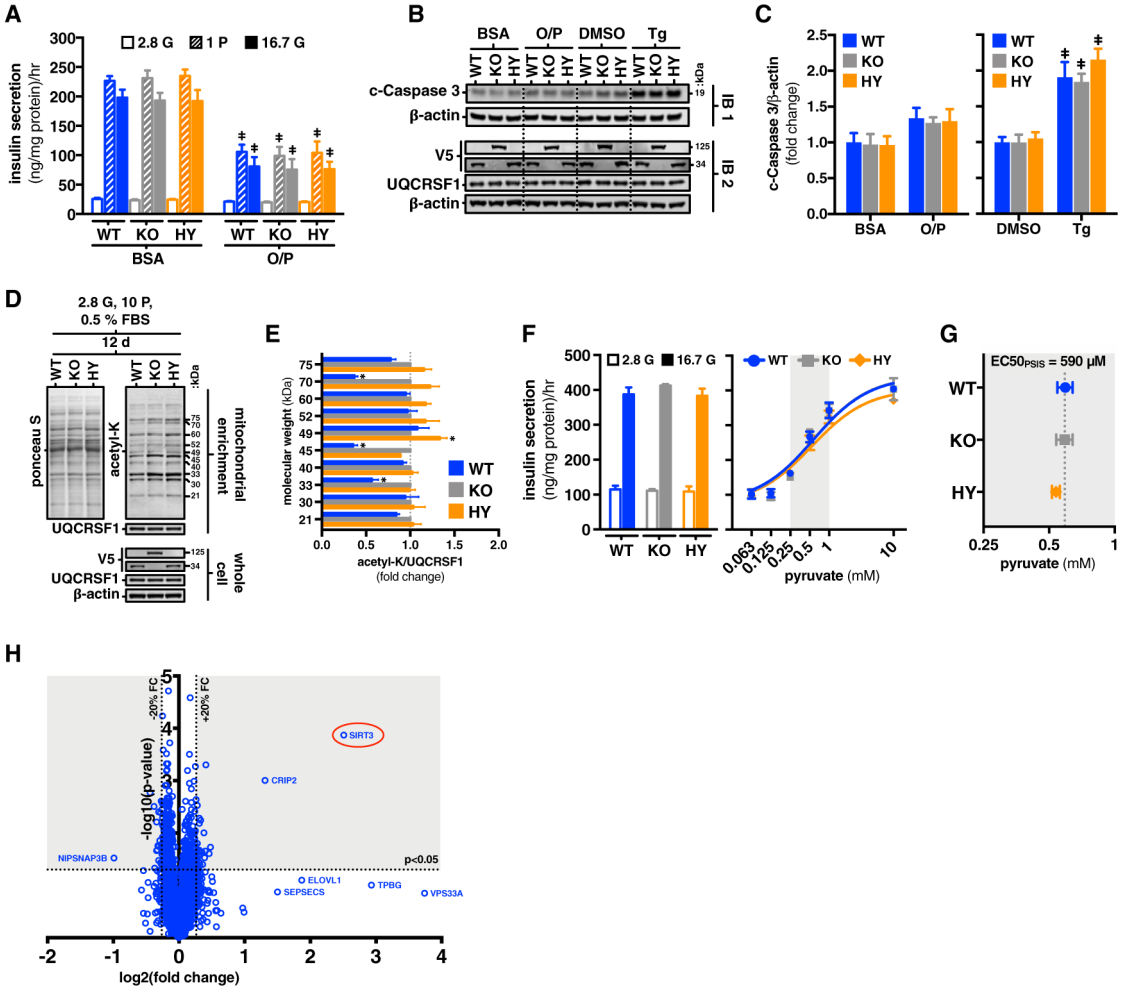

Figure 5. Changes in the SIRT3-Targeted β Cell Acetylproteome Do Not Affect Responses to Cell Stress Agents or Cause Global Changes in Protein Expression

(A) Insulin secretion in response to 2.8 mM glucose, 2.8 mM glucose supplemented with 1 mM pyruvate, or 16.7 mM glucose following 48-hr treatment with BSA control (BSA) or 0.5 mM 2:1 oleate/palmitate (O/P) conjugated to BSA. n = 3 independent experiments. (B) Immunoblot detection of cleaved caspase 3 (19 kDa) following 48-hr treatment with O/P versus BSA or DMSO versus 10 nM Thapsigargin (Tg). (C) Immunoblot quantification of cleaved caspase 3 expression relative to KO cells set to 1. n = 4 independent experiments. (D) Immunoblot detection of lysine acetylation (acetyl-K) in mitochondrially enriched fractions following 12-day culture at confluence in high-pyruvate medium. (E) Immunoblot quantification of lysine acetylation in mitochondrially enriched fractions relative to fractions from KO cells set to 1. n = 3 independent experiments. (F) Insulin secretion following 12-day culture at confluence in high-pyruvate medium. Left: GSIS in response to 2.8 and 16.7 mM glucose. Right: insulin secretion in response to 2.8 mM glucose supplemented with a range of pyruvate doses (63 μM–10 mM). Dose-response curves are nonlinear fit (agonist) versus response.

(G) EC_{50} of pyruvate response curves in (F). n = 3 independent experiments. Data represent means ± SE. Statistical comparisons were made using two-way ANOVA with Bonferroni's multiple comparisons test. ‡p ≥ 0.05 effect of treatment, *p ≥ 0.05 effect of cell line.
(H) Changes in expression of 5,897 proteins measured by mass spectrometry in mitochondrially enriched fractions of WT cells compared with KO cells plotted as Log2 fold change (x axis) and –Log10 p value (y axis). n = 3 independently prepared mitochondrial fractions.

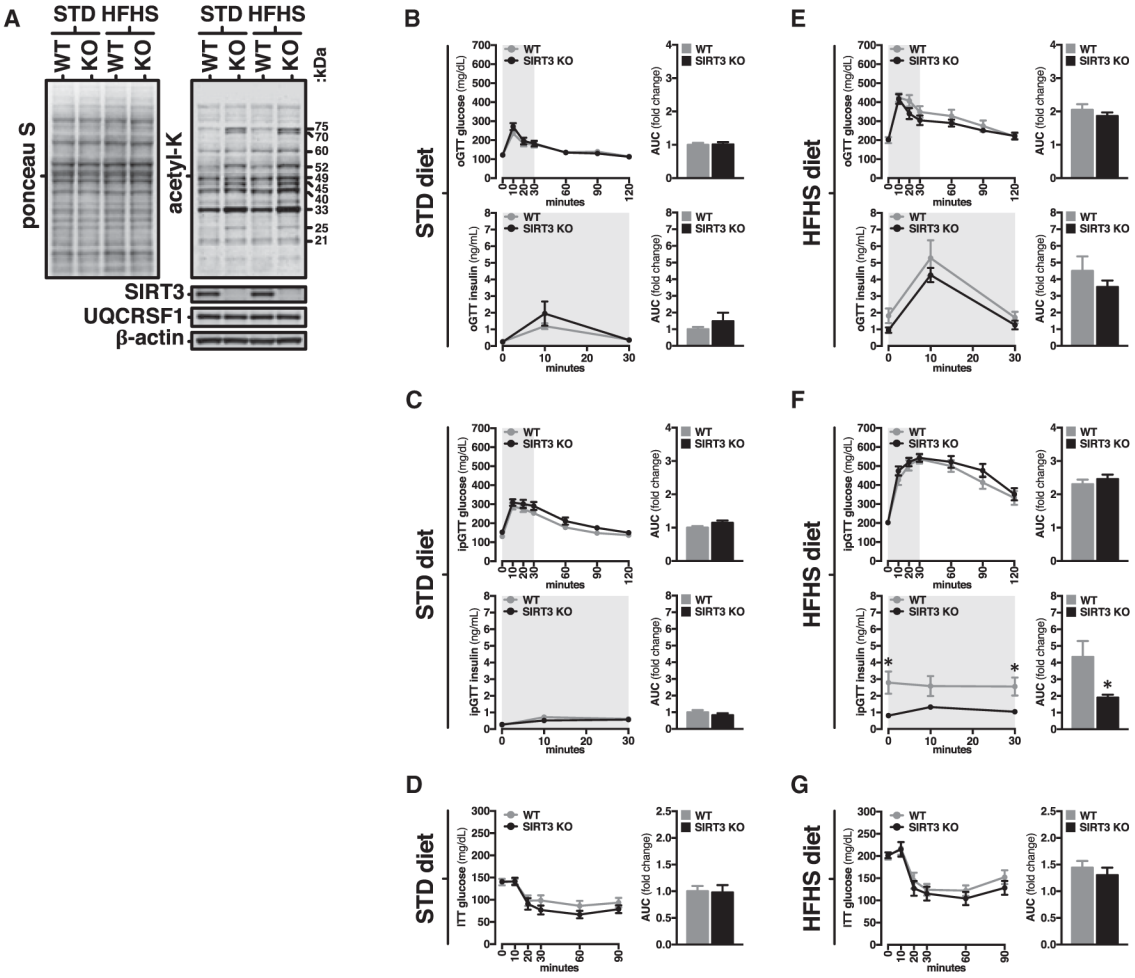

Figure 6. Protein Acetylation, GTTs, and ITTs in SIRT3 KO and Wild-Type Animals Fed on an STD or HFHS Diet

(A) Immunoblot detection of lysine acetylation and SIRT3 in pooled isolated islets from SIRT3 KO and wild-type mice fed on an STD or HFHS diet. n = 3–5 animals per group.

(B) Changes in glucose and insulin levels during an oral glucose tolerance test (oGTT) in STD diet-fed mice.

(C) Changes in glucose and insulin levels during an i.p. glucose tolerance test (ipGTT) in STD diet-fed mice.

(D) Changes in glucose levels during an insulin tolerance test (ITT) in STD-fed SIRT KO and wild-type mice. (E) Changes in glucose and insulin levels during an oGTT in HFHS diet-fed mice. (F) Changes in glucose and insulin levels during an ipGTT in HFHS diet-fed mice. (G) Changes in glucose levels during an ITT in HFHS diet-fed SIRT3 KO and wild-type mice. n = 10–14 animals per group. Relative area under the curve (AUC) for blood glucose and plasma insulin was calculated with STD diet-fed WT animals set to 1. Data represent mean ± SE. Statistical comparisons were made using two-way ANOVA with Bonferroni's multiple comparisons test. *p ≥ 0.05 effect of genotype.

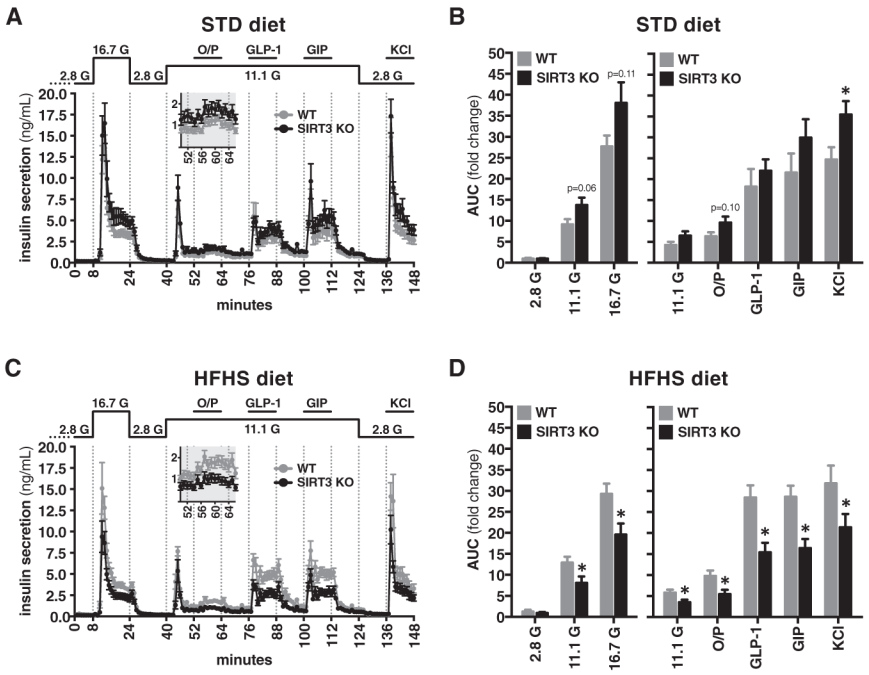

Figure 7. Perifusion of Islets from SIRT3 KO and Wild-Type Mice Fed STD or HFHS Diets

(A and B) Perifusion of islets isolated from STD diet-fed mice. The inset shows potentiation of GSIS by O/P. (B) AUC of the islet perifusion results shown in (A). (C and D) Perifusion of islets from HFHS dietfed mice (C). The inset shows potentiation of GSIS by O/P. (D) AUC of the islet perifusion experiment shown in (C). All islets treated with either 2.8, 16.7, and 11.1 mM glucose (11.1 G), 11.1 G + 0.5 mM O/P, 11.1 G + 0.03 nM GLP-1, 11.1 G + 0.3 nM GIP, or 2.8 mM glucose + 30 mM KCl. (A and C) Insulin samples collected at 1-min intervals. Chambers were loaded with 60 sizematched islets from a single animal. WT-STD, n = 8; SIRT3 KO-STD, n = 11; WT-HFHS, n = 10; SIRT3 KO-HFHS, n = 10. (B and D) Relative AUC for the islet perifusion insulin secretion response calculated with STD diet-fed WT animals set to 1. Data represent mean ± SE. Statistical comparisons of AUC analyses were made using two-way ANOVA with Bonferroni's multiple comparisons test. *p ≥ 0.05 effect of genotype.

KEY RESOURCES TABLE

REAGENT or RESOURCE	SOURCE	IDENTIFIER
Antibodies		
SIRT3	Cell Signaling Technology	Cat#2627
Total OXPHOS	Abcam	Cat#ab110413
V5	Thermo Fisher Scientific	Cat#MA5-15253
Citrate Synthase	Origene	Cat#TA308265
pan Acetylated-Lysine	Cell Signaling Technology	Cat#9441
UQCRSF1	Abcam	Cat#14746
β-actin	Cell Signaling Technology	Cat#8457
Caspase 3	Cell Signaling Technology	Cat#9662
IRDye 800CW	Li-COR	Cat#926-32213
IRDye 680RD	Li-COR	Cat#926-68072
Plasmids for Lentivirus Construction		
pLenti6.3/hSIRT3 WT-V5	This paper	N/A
pLenti6.3/V5-GW/lacZ	Thermo Fisher Scientific	Cat#V53306
pLenti6.3/hSIRT3 N229A-V5	This paper	N/A
pLenti6.3/hSIRT3 H248Y-V5	This paper	N/A
pLenti6.3/hSIRT3 NA/HY-V5	This paper	N/A
Chemicals, Peptides, and Recombinant Proteins		
TransIT-LT1	Mirus Bio	Cat#2300
Geneticin (G418)	Thermo Fisher Scientific	Cat#10131035
Puromycin	Thermo Fisher Scientific	Cat#A1113803
Blasticidin	Thermo Fisher Scientific	Cat#A1113903
Thapsigargin	Thermo Fisher Scientific	Cat#T7459
Halt Protease Inhibitor Cocktail	Thermo Fisher Scientific	Cat#78430
Critical Commercial Assays		
STELLUX Chemi rodent insulin ELISA kit	ALPCO	Cat#80-INSMR
AlphaLISA Biomarker Detection Kit	PerkinElmer	Cat#AL350
10-plex Tandem Mass Tag (TMT) reagent kit	Thermo Fisher Scientific	Cat#90110
iScript cDNA Synthesis Kit	Bio-Rad	Cat#1708890
iTaq Universal SYBR Green Supermix	Bio-Rad	Cat#172-5120
TaqMan Gene Expression Assay for *hINS*	Thermo Fisher Scientific	Cat#4331182
Deposited Data		
Raw LC-MS/MS data	ProteomeXchange Consortium via the PRIDE partner repository	PXD009509
Experimental Models: Cell Lines		

REAGENT or RESOURCE	SOURCE		IDENTIFIER
Rattus norvegicus: INS-1 832/13	In house	N/A	
Rattus norvegicus: WT (polyconal set 1)	This paper	N/A	
Rattus norvegicus: KO (polyconal set 1)	This paper	N/A	
Rattus norvegicus: NA (polyconal set 1)	This paper	N/A	
Rattus norvegicus: HY (polyconal set 1)	This paper	N/A	
Rattus norvegicus: DM (polyconal set 1)	This paper	N/A	
Rattus norvegicus: WT (polyconal set 2)	This paper	N/A	
Rattus norvegicus: KO (polyconal set 2)	This paper	N/A	
Rattus norvegicus: NA (polyconal set 2)	This paper	N/A	
Rattus norvegicus: HY (polyconal set 2)	This paper	N/A	
Rattus norvegicus: DM (polyconal set 2)	This paper	N/A	
Experimental Models: Organisms/Strains			
Mus musculus: Sirt3$^{+/+}$: C57BL/6J/*Nnt* wild-type	This paper		N/A
Mus musculus: Sirt3$^{-/-}$: C57BL/6J/*Nnt* wild-type	This paper		N/A
Oligonucleotides			
Sirt3-directed gRNA 1 (pair 1): ACATTGGGCCTGTAGTGCCC	This paper		N/A
Sirt3-directed gRNA 2 (pair 1): CCTTCGGCTGCTTCACGACA	This paper		N/A
Sirt3-directed gRNA 1 (pair 2): GCTTCAACCAGCTTTGAGGC	This paper		N/A
Sirt3-directed gRNA 2 (pair 2) CTACGTGCACGGTCTGTCGA	This paper		N/A
hSIRT3 WT fusion protein w/ attR1 & attR2 sites	IDT		N/A (custom)
See Table S4 for qPCR Primer Sequences			
Recombinant DNA			
pSpCas9n(BB)-2A-Puro (PX462)	Ran et al., 2013		Addgene #48141
PX462/*Sirt3*-directed gRNA 1 (pair 1)	This paper		N/A
PX462/*Sirt3*-directed gRNA 2 (pair 1)	This paper		N/A
PX462/*Sirt3*-directed gRNA 1 (pair 2)	This paper		N/A
PX462/*Sirt3*-directed gRNA 2 (pair 2)	This paper		N/A
pDONR221	Thermo Fisher Scientific		Cat#12536017
pDONR221/hSIRT3 WT	This paper		N/A
pDONR221/hSIRT3 N229A	This paper		N/A
pDONR221/hSIRT3 H248Y	This paper		N/A
pDONR221/hSIRT3 NA/HY	This paper		N/A
Software and Algorithms			
Proteome Discoverer v2.2 (PD2.2)	Thermo Fisher Scientific		N/A
PRIDE partner repository accession number	ProteomeXchange		PXD009509